TECHNICAL MEMORANDUM

180

Development of a high resolution semi Lagrangian version of the ECMWF forecast model

A.J. Simmons

Research Department

August 1991

European Centre for Medium-Range Weather Forecasts
Europäisches Zentrum für mittelfristige Wettervorhersage
Centre européen pour les prévisions météorologiques à moyen

Development of a high-resolution, semi-Lagrangian version of the ECMWF forecast model

Document presented to the 19th Session of the Scientific Advisory Committee, 1991.

1. INTRODUCTION

In its four-year plan for the period 1989-1992, ECMWF proposed development of a high-resolution version of its forecast model for operational implementation in late 1990. It also proposed the acquisition of a computer at least six times more powerful than its CRAY X-MP machine on which to run the new version of the model. A target resolution of T213 in the horizontal and 31 levels in the vertical (T213/L31) was indicated, entailing a doubling of horizontal resolution, and an approximate doubling of vertical resolution between the boundary layer and stratospheric model levels. Support for this plan was provided by the encouraging results of forecast experiments at T159/L19, T213/L19 and T63/L31 resolutions (*Simmons et al.*, 1987; *Simmons and Dent*, 1989). Data assimilation tests using the T63/L31 resolution showed a further advantage of the improved vertical structure of the model. The 19- and 31-level resolutions are illustrated in Fig. 1[1].

The proposed increase in computational power by a factor of at least six was based on an estimate of a 12-fold increase in the cost of the new model version over that of the then-operational T106/L19 version, coupled with the possibility of devoting a higher proportion of the available computing power to the production of the operational forecast. However, in implementing the plan, it became evident that the required power could not be provided on the time scale envisaged, and in July 1990 experimental use began to be made of a CRAY Y-MP8 computer offering between three and four times the power of its predecessor. Moreover, it soon became clear that the enhancement by a factor of 12 for the T213/L31 model was a serious underestimate. The principal cause of this was an unexpectedly severe timestep limitation due to the CFL criterion for the computational stability of the vertical advection scheme. A contributing factor was the change in parametrization in May 1989, which both increased the direct cost of the model and increased typical vertical velocities.

[1]The 31-level distribution currently used, and illustrated in Fig. 1, differs slightly from that used for the earlier experimentation. The top four, rather than two, layers are now layers of constant pressure.

Two significant gains in the computational efficiency of the model have nevertheless enabled a T213/L31 version to be developed for operational forecasting on the CRAY Y-MP8. The first is a reduction in the computational grid of the model, following the work of *Machenhauer* (1979). This gives a resolution in physical space which is approximately uniform over the globe, and results in an important saving in secondary memory requirements in addition to a saving in computation time. A more major saving in time comes from adopting the semi-Lagrangian method for the treatment of advection pioneered by *Robert* (1981). Code reorganization necessitated by the latter also enabled a more efficient calculation of Legendre transforms, and a small reduction in the primary memory requirement of the model.

The following two sections of this paper summarize the development of the reduced grid and semi-Lagrangian version of the model. Section 4 presents results of forecast experiments carried out at T213/L31 resolution, and section 5 discusses pre-operational trials in which the new version was used in data assimilation as well as forecast mode. Conclusions are presented in section 6.

2. THE REDUCED GRID

Tests of the use of the reduced Gaussian grid at T106 resolution have been reported by *Hortal and Simmons* (1991). A saving in excess of one-third the number of points covering the globe was obtained by increasing grid-lengths in the zonal direction under the conditions that they did not exceed the grid-length at the equator, and that the number of points around each latitude circle enabled use of a fast Fourier transform. Results showed that such a grid could be used for global forecasting (and presumably also for climate studies) with no significant loss of accuracy compared with use of a conventional grid uniform in longitude. Such differences as did occur appeared to be principally due to differences in the model orographies and sub-gridscale orographic variances computed for the new and conventional grids. A saving in computational time of around 22% was found for T106/L19 resolution.

The reduced grid chosen for T213 resolution is illustrated over Europe in Fig. 2. Initial testing at this resolution was carried out using 19 levels and the original Eulerian version of the model. Twelve cases spread throughout the year were chosen, and comparison was made with corresponding full-grid forecasts. The saving in computation time was 27% with the reduced grid. Objective verification scores showed that the two sets of forecasts were virtually identical in quality. An example of day-5 500hPa heights is presented in Fig. 3 to illustrate this. Fig. 4 shows corresponding distributions of precipitation over part of southern Europe, including the T106/L19 forecast for comparison. For purposes of plotting, output on the reduced grid has been interpolated linearly to the full grid before contouring, and this inevitably introduces some smoothing of the rainfall field. The two T213 forecasts are, however, very much closer to each other than

to the T106 forecast. The extra detail in the higher resolution forecasts verifies well in this case (*Simmons and Dent*, 1989).

In view of the success of the reduced grid in these tests, provision for using it was built into the semi-Lagrangian version of the model then under development. This involved some increase in computation in the interpolation stage of the model, but its cost was more than compensated by the extra savings resulting from the higher proportion of the overall calculation that is carried out in grid-point space for the semi-Lagrangian scheme. Initial testing gave satisfactory results for the most part, but noise was evident in vorticity and surface-pressure fields in polar regions for some flow orientations. This was traced to the representation of the cancellation between the two pressure-gradient terms near the Greenland and Antarctic plateaux, and occurred also in the "u-v" Eulerian formulation (see *Ritchie*, 1988) developed in conjunction with the semi-Lagrangian version. It was largely corrected by reverting to the use of additional zonal wavenumbers in the spectral/grid-point transforms, adopting what is referred to in *Hortal and Simmons* (1991) as the "fully reduced grid" rather than the "fully reduced model". As a small amount of noise remained in the immediate vicinity of the poles in subsequent semi-Lagrangian tests, the number of points used at the three most northerly and southerly latitudes was increased from 6,12 and 18 to 12,16 and 20. These changes had little impact on the computational cost of the model, and a quite negligible impact on the quality of the forecasts apart from removal of the noise.

3. THE SEMI-LAGRANGIAN SCHEME

3.1 Formulation

The semi-Lagrangian scheme that has been adopted is a natural extension of the work of *Ritchie* (1987, 1988, 1991) in applying the technique to spectral models. It preserves, however, as much as possible of the vertical discretization of the original Eulerian hybrid-coordinate model (*Simmons et al.*, 1989), and this discretization is retained in full in the Eulerian "u-v" option which has been included in the new model code. In developing the semi-Lagrangian approach to the point of operational implementation, attention was devoted to three aspects. These were the basic formulation, the introduction of approximations of acceptable accuracy, and the production of an efficient computer code. A working scheme has been produced, but future refinements are likely.

Full details of the scheme will not be given here. It uses three time levels and an interpolating treatment of the three-dimensional advection, converting to tangential Cartesian coordinates for the updating of the wind fields. Vertical velocities are calculated in a way similar to that used in the conventional Eulerian scheme. The semi-Lagrangian treatment of the continuity equation is formulated so as to allow $\ln(p_s)$ to be retained

as a prognostic model variable, following in part ideas developed within the HIRLAM project (*Haugen and McDonald*, personal communication).

Noise characteristics of the scheme were found to depend sensitively on the evaluation of the right-hand side terms of the governing dynamical equations. The best results obtained to date were achieved by calculating the momentum-equation terms as averages of values at the beginning and end points of the trajectories, but calculating the temperature- and continuity-equation terms at the mid-points. The semi-implicit treatment of gravity-wave terms is applied as a correction in a way similar to that in the previous Eulerian version. An $O(\Delta t)$ term formed by taking half the difference between linearized gravity-wave tendencies at time levels t and $t-\Delta t$ is added at the departure point, and the corresponding term formed from time levels t and $t+\Delta t$ is added at the grid-point that is the end of the trajectory. The additional scaling factor of 0.75 used previously (*Simmons et al.*, 1989) is no longer included, as it was found to give rise to noise along a strong ($\sim 110 ms^{-1}$) jet stream in one case.

Changes due to parametrized physical processes are computed at model grid points after completion of the grid-point dynamical calculations (including the semi-Lagrangian advection) and prior to transformation to spectral space. It was found necessary to include implicit treatments for gravity-wave drag and convective momentum transfer, as already used for boundary-layer diffusion. This was to ensure stability when using the longer timesteps made possible by the semi-Lagrangian scheme. The artificial enhancement of horizontal diffusion at upper levels and in cases of strong wind used to ensure computational stability of the Eulerian version of the model was removed for testing of the semi-Lagrangian scheme. Also, the time filtering parameter was increased from 0.1 to 0.2 for semi-Lagrangian forecasts. The longer timesteps used for these forecasts are such that this does not imply an increase in damping of meteorological modes.

The semi-Lagrangian method introduces an element of additional smoothing into the model, associated with the interpolation of fields to departure points. This was found to be small in practice. Some reduction in the intensity of localized strong vertical motion in the tropics was seen in testing, but this was associated principally with the use of a longer timestep rather than the semi-Lagrangian technique.

Experimentation with the formulation of horizontal diffusion was nevertheless undertaken in the development of the T213/L31 version of the model. The basic horizontal diffusion used in the T106/L19 operational model is a linear, fourth-order scheme with an e-folding time of about 3 hours for the smallest resolved scale. This diffusion is enhanced by a factor of 2.5 for the divergence field. To damp vertically propagating gravity waves in the stratosphere, diffusion is increased progressively by a factor of 2 at each level from level number 5 (around 100hPa) to level number 2 (30hPa). T213 experiments initially used the same fourth-order

scheme, but with one-hour e-folding time, and diffusion of divergence enhanced by a factor of 3. This was replaced by a sixth-order scheme with an e-folding time of 15min on the smallest resolved scale, and no enhancement for the divergence field. For fields other than divergence, this gives a reduction in damping by factors of about 5 for wavenumber 106 and 15 for wavenumber 63 compared with the scheme used for T106. For the 31-level vertical resolution, the increase in diffusion at upper levels is by a factor of $\sqrt{2}$ applied from level 9 (around 190hPa) to level 2 (30hPa).

The principal cost of the semi-Lagrangian scheme is in the interpolation stage, and effort has been devoted to establishing a scheme with acceptable accuracy at minimum cost, and to coding in an efficient way. Linear interpolation is used in the calculation of trajectories (which employs a single iteration) and in the evaluation of terms at the mid-points of these trajectories. A mixed cubic/linear interpolation suggested by *Courtier* (personal communication) is used for terms evaluated at departure points.

A new scanning structure has been adopted, in the first place to avoid a substantial increase in the memory requirement of the model. As a byproduct, it was possible to implement a more efficient execution of the Legendre transforms, and to ensure reproducible results without a multi-tasking overhead. Other ways of improving the efficiency of the Legendre transforms were found, and the number of transforms is reduced by use of the semi-Lagrangian scheme. Thus the Legendre transforms account for about 13% of the cost of the T213/L31 semi-Lagrangian model, compared with 19% in the operational T106/L19 code. This partly compensates for the increased cost of the semi-Lagrangian scheme itself, so that at T213/L31 resolution the cost of a non-radiation semi-Lagrangian timestep is less than 20% higher than with the original Eulerian code. The multi-tasking speed-up of the new version using 8 processors is 7.5, which compares well with the figure of 7.3 obtained originally on the CRAY Y-MP8 at T213/L19 resolution.

3.2 Performance

A limited number of tests of the original Eulerian version at T213/L31 resolution showed that a 4-minute timestep could not be used, and that a 3-minute timestep gave stable integrations. All cases run with the current semi-Lagrangian formulation have been stable with a 20-minute timestep. The elapsed time of a 10-day forecast without post-processing has been reduced from more than 24 hours with the standard Eulerian code to about 4 hours by the combined use of the reduced grid and semi-Lagrangian code.

Experimental results providing a completely rigorous comparison between Eulerian and semi-Lagrangian forecasts at T213/L31 resolution are not available. Some parametrization changes were made in the course of development of the semi-Lagrangian version, and it has not been feasible to rerun earlier Eulerian forecasts as their costly execution was possible only because of a low workload on the CRAY Y-MP soon after

installation. Nevertheless, the Eulerian and semi-Lagrangian forecasts are sufficiently close that it appears that there are no serious disadvantages to use of the semi-Lagrangian method and 20-minute timestep for T213/L31 resolution.

As an example, Fig. 5 presents 5-day 500hPa height forecasts and the verifying analysis for a case in which there was a marked difference between T106/L19 and T213/L31 forecasts over Europe. Differences between the Eulerian and semi-Lagrangian forecasts shown for T213/L31 are evidently much smaller than differences between either of these forecasts and the T106/L19 forecast. This case also serves as an example of a significant improvement in forecast accuracy due to use of the higher resolution.

Eulerian and semi-Lagrangian T213/L31 forecasts of 10m winds at one-day range are shown in Fig. 6. The point here is not to attempt comparison with a corresponding T106/L19 forecast or with reality, but rather to draw attention to the similarity of the two wind fields. In particular, there is no indication that use of the semi-Lagrangian scheme and longer timestep gives any significant smoothing of the high-resolution detail.

A parametrization change was required to obtain the very close agreement noted above. Independent work reported by *Janssen et al.* (1991) had identified a time-truncation error in the parametrization of boundary-layer diffusion which caused low-level winds to be generally stronger in T106/L19 Eulerian forecasts with the usual 15-minute timestep than in forecasts with much shorter timesteps. The error arose because the time-split implicit solution used for the boundary-layer parametrization did not successfully preserve the balance between the resolved dynamical forcing and the turbulent diffusion. The semi-Lagrangian model, and the alternative "u-v" Eulerian version, produce full dynamical tendencies in grid-point space which are not available in the original Eulerian code. The time-truncation error is reduced by incorporating these dynamical tendencies in solving the equations for the diffusive boundary-layer tendencies. This was used in the semi-Lagrangian forecast shown in Fig. 6. Its impact can be seen in Table 1, which shows that in the absence of the revised boundary-layer treatment, mean low-level winds from the T213/L31 forecast with 20-minute timestep are closer to those from the 15-minute timestep T106/L19 forecast than to those from the 3-minute timestep T213/L31 forecast.

Mean 10m wind speeds (ms^{-1}) D + 24h from 15 April 1990					
			Global	Land	Sea
T106/L19	EUL	Δt = 15 min	6.1	4.0	6.9
T213/L31	EUL	Δt = 3 min	5.8	3.6	6.7
T213/L31	SL	Δt = 20 min	6.2	4.3	7.0
T213/L31	SL	Δt = 20 min	5.8	3.5	6.7

(Non-split vertical-diffusion scheme)

Table 1 : Mean 10m wind speeds averaged globally, and separately over land and sea, for a standard T106/L19 Eulerian forecast and various T213/L31 forecasts.

Information on the mass conservation of the semi-Lagrangian forecasts is provided in Table 2, which shows the spurious change in global-mean pressure over the 10-day forecast range for eight cases run with the T213/L31 semi-Lagrangian version and with the original T106/L19 model. Mass conservation is poorer in the semi-Lagrangian version than in the Eulerian version when the comparison is made at a fixed resolution, but conservation improves with increasing resolution. Table 2 suggests that for the majority of cases the T213/L31 semi-Lagrangian model conserves mass better than the T106/L19 Eulerian model. The exception occurs for the (northern-hemispheric) mid-winter months. The poorer mass conservation found in forecasts from dates within these months did not occur generally in earlier forecasts in which there were differences in the semi-Lagrangian formulation, but these forecasts exhibited a higher level of noise near orography, and one became unstable. This nevertheless suggests that a change in formulation which gives better conservation may be found in the future.

Global-mean surface pressure change (hPa) (Day 10) - (Day 0)		
Initial date	T106/L19 Eulerian	T213/L31 Semi-Lagrangian
15/04/90	.14	-.01
01/06/90	.15	-.02
15/07/90	.18	-.11
01/09/90	.13	-.05
15/10/90	.18	-.02
15/12/90	.18	-.21
15/01/91	.12	-.34
15/02/91	.05	-.30

Table 2 : A comparison of mass conservation between the standard T106/L19 Eulerian model and the new T213/L31 semi-Lagrangian model. The change over ten-day runs in the global-mean surface pressure is illustrated for forecasts from the eight dates shown.

At T213/L31 resolution, contours of the 500hpa height field commonly exhibit small-scale ripples where the flow crosses steep orography. This occurs in a largely similar way in both Eulerian and semi-Lagrangian versions of the model, but amplitudes are slightly larger in the semi-Lagrangian forecasts. A much weaker effect can also be discerned in T106/L19 forecasts. Study of cross-sections in a particularly well-marked case over the Rockies reveals the presence of pronounced orographically forced gravity waves in the higher resolution forecast. The realism of the model behaviour in this case is to be assessed by comparison with limited-area model simulations of much higher horizontal and vertical resolution.

4. FURTHER COMPARISONS OF T213/L31 AND T106/L19 FORECASTS

In this section we present a sample of results from a series of forecast experiments carried out to establish the stability and meteorological performance of the semi-Lagrangian model at T213/L31 resolution. Forecasts were run from initial dates spanning all seasons. The initial datasets were created by interpolating operational T106/L19 analyses.

The results show a quite general improvement in synoptic detail in the early medium range. A clear example of this is seen in the comparison of the T213/L31 and T106/L19 forecasts of mean sea-level pressure for day 3 shown in Fig. 7. The maps show that the higher resolution forecast is much more successful in capturing the pattern of three lows near the Greenwich meridian. Also, the intensities of the lows elsewhere on the map are more accurately depicted in the T213/L31 forecast.

Fig. 8 shows T106/L19 and T213/L31 forecasts of 10m wind at the 3-day range for another case. There is an expected increase in detail in local wind systems in the higher-resolution forecast, for example the sharp orographically-induced gradient in wind speed in the flow north of Majorca. There are also some pronounced differences in flow direction and speed over the seas surrounding Italy. Verification is presented in Fig. 9 in terms of the operational T106/L19 analysis (which is incapable of describing the local flow detail seen in the T213/L31 forecast) and the SYNOP wind reports. For the most part the T213/L31 forecast appears to be the more accurate of the two. Predicted rainfall totals for the preceding 24 hours are presented in Fig. 10, and show substantial differences. The corresponding observations are plotted in Fig. 11, and provide confirmation of the superiority of the higher resolution forecast.

It becomes increasingly difficult to assess performance differences at longer time ranges. Some of the difficulties are illustrated in Fig. 12, which shows 5-day forecasts of 1000hPa height, the verifying analysis, and differences between the T106/L19 and T213/L31 forecasts. Moving around the hemisphere, we see that the two forecasts are equally poor in positioning a low over Japan, but that the intensity of this tropical storm is, not surprisingly, stronger for T213/L31. The simulated storm is in fact a grossly-misplaced

representation of an actual storm named "Yancy", which in the analysis is centred off the edge of the map near 120°E. The higher resolution forecast is clearly the better in the representation of the major depression near the dateline, and to a lesser extent in the low over northwest Canada. It is poorer in its production of a low near Newfoundland. In the European region, a low is centred over Denmark in reality. The T106/L19 forecast shows no evidence of the development of such a system, whereas the T213/L31 version has evidently produced a strong low, but one which is not positioned correctly.

Objective verification in this case is shown in Fig. 13 for the extratropical northern hemisphere as a whole, and separately for Europe. At day 5, the T213/L31 forecast appears somewhat worse for the hemisphere, and substantially worse for Europe. It is highly questionable as to whether this is a true reflection of the performance of the two models.

Plots of the evolution of eddy kinetic energy for the extratropical northern hemisphere are presented in Fig. 14 for a sample of six cases. In each, a higher level of eddy energy is seen to occur for the T213/L31 forecast than for T106/L19. Comparison with analyses does not give a uniform picture as to which is better, since in some cases the higher resolution forecast still represents an underestimate of reality, whereas in others it provides an overestimate, particularly towards the end of the 10-day range.

A greater activity for the new version of the forecast model is seen also in precipitation statistics. Global-mean precipitation rates are given in Table 3 for two initial dates, and five model configurations. These have resolutions T106/L19, T106/L31 and T213/L31, and we show results for three versions of the parametrizations. Cycle 38 denotes the version used operationally with T106/L19 since April 1991, apart from the changed implicit treatments used in the semi-Lagrangian version employed for the T106/L31 (Δt=30min) and T213/L31 runs. Cycle 39 is a newer version, with changes in the treatments of cloud and radiation, chosen for the final testing of T213/L31 (and used in the forecasts discussed earlier in this section). Also included for comparison in the table are results for T106/L19 using cycle 36 of the model, the version operational at the date of each forecast.

The precipitation rates shown in Table 3 illustrate how the increase in vertical resolution, the increase in horizontal resolution, and the parametrization change from cycle 38 to cycle 39 each tend to increase precipitation, giving a net increase of some 15%. The increase occurs in both convective and resolved large-scale components. Similar results are found in other cases. Note, however, that when comparison is made with the cycle 36 version of T106/L19, the version using the parametrizations operational until April 1991, the increase in precipitation with the new version of the model is only of the order of 5%.

GLOBAL-MEAN PRECIPITATION RATE (mm/day 10-day mean)		
	90/7/15	91/1/15
T106/L19 cycle 38	2.75	2.64
T106/L31 cycle 38	2.89	2.79
T213/L31 cycle 38	2.96	2.85
T213/L31 cycle 39	3.16	3.01
T106/L19 cycle 36	3.00	2.87

GLOBAL-MEAN CLOUD COVER (% day 5)		
	90/7/15	91/1/15
T106/L19 cycle 38	53	53
T106/L31 cycle 38	59	61
T213/L31 cycle 38	58	60
T213/L31 cycle 39	56	59
T106/L19 cycle 36	58	59

Table 3 : Global-mean precipitation and cloud cover for five model configurations and two initial dates.

Corresponding figures for the cloud cover are also given in Table 3. A sharp increase occurs with the increase in vertical resolution. This is compensated partly by the increase in horizontal resolution, and further by the parametrization change. Cloud cover nevertheless remains higher than in the latest operational T106/L19 version of the model. Much of the increase is in the low cloud, and may be associated with the sharper inversions that occur at the better-resolved top of the planetary boundary layer. The decrease due to higher horizontal resolution is seen in narrower bands of frontal cloud. Again, the results from T213/L31 using cycle 39 parametrizations are closer to those from the cycle 36 version of T106/L19 than to those from the cycle 38 version.

We conclude this section with two figures relating to objective verification of an ensemble of 15 cases. T213 and T106 fields were both truncated to T63 for the purposes of this verification. Fig. 15 presents a scatter plot showing anomaly correlations of 1000hPa height for the extratropical northern hemisphere from T213/L31 and T106/L19 forecasts. Both used cycle 38 parametrizations, but adiabatic initialization was used for the higher resolution forecasts as the diabatic scheme had not been incorporated in the semi-Lagrangian version at the time the forecasts were carried out. The improvement due to increased resolution is clear.

Mean 500hPa height scores are shown in Fig. 16. Beyond day 4 the higher resolution forecasts appear poorer when the average is taken over all cases (upper panel), although the difference is small while the mean anomaly correlation remains above 60%. Moreover, the two sets of forecasts show little separation when the

average only includes cases in which correlations are above 60% for both forecasts(lower panel). As forecast quality diminishes, the higher eddy energy of the T213/L31 model presumably contributes to a drop in forecast skill scores relative to T106/L19.

The cases included in Figs. 15 and 16 have been repeated using cycle 39 parametrizations, and a further 12 cases have been run with this version. Results show a substantial improvement in tropical verification in the medium range, an expected consequence of the parametrization change, but a slight deterioration in the extratropical northern hemisphere. However, the T213/L31 forecasts used diabatic initialization for these cases, and it was subsequently discovered that results were corrupted by a multi-tasking error in the accumulation of the diabatic forcing. The additional cases nevertheless served to provide reassurance of the stability of the T213/L31 version with the 20-minute timestep.

5. A PARALLEL RUN

Technical development of the new model, and its incorporation in the data assimilation system, had reached the point early in June 1991 that a run of the T213/L31 system in parallel with the operational T106/L19 system could begin. Data assimilation with the high resolution model began on 11 June, and forecasts were carried out daily from 18 June. Although some encouraging synoptic features were observed in the early forecasts, it soon became evident that performance of the new system was very much poorer than had been expected. Errors were successively found in the initiation of the tidal history file, the specification of albedo and in the multitasking of the diabatic initialization. Only with correction of the latter, for forecasts from dates starting 11 July, were representative results obtained. The earlier forecasts nevertheless provided further evidence as to the stability of the model. The parallel running of forecasts continued until halted for the summer vacation period on 28 July. The new data assimilation system was run for a further week to provide consistent analyses for verification.

In this section we thus discuss results from the two sets of 18 forecasts that were run at T213/L31 and T106/L19 resolution from 12UTC each day from 11 to 28 July 1991. It should be stressed that the assessment of these forecasts is far from complete, and also that they relate to just one period of the year. Also, although the terminology T213/L31 is used to identify the new model version, the inclusion of the accompanying change in parametrization should not be forgotten.

We present first a series of synoptic maps of the 500hPa height field. Fig. 17 displays two- and five-day forecasts for 12UTC 23 July, and the two analyses for this time. The latter can be seen to be extremely similar. This case was chosen as it provides a prime example of the better representation of features in high latitudes by T213/L31 that was evident for much of the period of the parallel run. In particular the vortex

centred over northern Canada is much weaker than in reality in the two-day operational forecast, and completely missing in the five-day forecast. Its intensity is well-captured in the two-day T213/L31 forecast, and slightly overestimated at day 5. The positional errors in these forecasts do not appear to be particularly large. However, by day 5 they are such that point forecast errors are in fact as large for T213/L31 as for T106/L19 at places in the vicinity of the vortex, despite its more accurate synoptic development.

Looking elsewhere on the maps shown in Fig. 17, the amplitudes of synoptic systems can be seen to be generally greater for the higher resolution model. This is for the most part beneficial at day 2, but the situation is far less clear at day 5. T213/L31 gives a better position to the trough approaching Ireland in the two-day forecast, but a poorer position in the five-day forecast.

Corresponding maps for five days earlier are presented in Fig. 18. Here the tendency for deeper lows with T213/L31 is seen to detrimental effect in the treatment of the system near Hudson Bay, with particularly poor positioning and gradients in the two-day forecast. The new model is seen to better effect in the European sector.

Also of interest in Fig. 18 are the analysis differences near the pole. These analyses are of interest in that they provided the initial conditions for the five-day forecasts which were seen to be very different at high latitudes in Fig. 17. There seems little doubt that it is the experimental analyses that are the better around this time. Not only do they yield better forecasts, but they are in closer agreement with the TOVS retrievals (which were not used below 100hPa in either analysis). Moreover, study of sequences of potential vorticity maps for the 315 and 330K isentropic surfaces reveals a much more consistent picture for T213/L31. Forecasts at this resolution tend to preserve well the amplitude of features in these fields, whereas there is a clear tendency for these amplitudes to diminish with increasing forecast range in the T106/L19 version of the model. During the period in question, anomalies in the potential vorticity distribution moved around the polar cap in a region where there are few observations available to the analysis in the absence of use of temperature retrievals. The general success of the T213/L31 system at high latitudes appears to be a consequence of the model's better representation of this process.

Fig. 19 shows a similar set of maps, but this time for five days after the date shown in Fig. 17. By this time the operational system was performing better in its handling of the high-latitude vortices. These can be seen still to be rather underestimated at the T106/L19 resolution, but by no more than the overestimation that occurs for T213/L31. The lows are, nevertheless, better positioned in the higher resolution forecasts.

Perhaps of more interest in Fig. 19 are the differences at five-day range over Europe. Here the T213/L31 system is significantly more accurate in capturing the onset of a blocking pattern. It is better in its prediction of the cut-off low over southern Europe, and in its positioning of southwesterly to westerly flow over the northern Nordic countries. Caution must be exercised in interpreting one such result from a parallel run of limited duration, but the generally higher level of eddy activity found for the T213/L31 model may indeed be more conducive to the establishment of blocks, under-prediction of which has been a longstanding forecast deficiency.

Examination of weather parameters shows that T213/L31 gives an improved fit of 2m temperatures to surface observations over Europe as a whole, although there are regions such as the Alps where the higher orography of T213 increases a cold bias. There is less of an under-prediction of cloud cover with the new version of the model. Patterns of precipitation from T213/L31 appear often to agree better with observations than those from T106/L19. An exception occurs early in the forecast range. Here T106/L19 has a tendency to produce too widespread and too intense rainfall, especially over higher ground. This tendency is clearly worse in the new version of the model. It can be seen in the global-mean components of the hydrological budget, as illustrated for one particular forecast in Fig. 20. The figure shows not only a general increase in precipitation of the order found in earlier forecast experiments, but also that the increase (which occurs predominantly over land) is not matched by a corresponding increase in evaporation, resulting in a much larger imbalance in the hydrological budget during the first half of the forecast range. Though a subject of concern and further investigation, this problem is likely to have been seen at its worst in this parallel run. The forecast experiments carried out for other seasons from interpolated T106/L19 analyses, and a T213/L31 data assimilation for a period within January 1991, exhibit much less excess precipitation at short range.

We now discuss some results from objective verification against analyzed fields. As before, results from both model versions are truncated to T63 prior to the evaluation of skill scores, and unless otherwise stated the T213/L31 forecasts are verified whenever possible against the T213/L31 analyses, and the T106/L19 forecasts are verified in all cases against the T106/L19 analyses. The ensemble-mean results to be presented must be treated with caution, not only as they come from one particular time of the year, but also because in these experiments there is a much greater sensitivity to the model change than in the earlier experiments in which all forecasts were from T106/L19 analyses. The sample of forecasts available for verification is not large enough to give a generally reliable measure of mean improvement.

Anomaly correlations of the 1000hPa height field largely reproduce the picture presented in Fig. 15 for the earlier experiments. In the parallel run there is more scatter across the diagonal, and a somewhat larger mean improvement. In contrast with the earlier results, the 500hPa height correlations now show a small mean

improvement in the medium range out to about day 7. This occurs for both hemispheres, as can be seen in Fig. 21. Corresponding standard deviations of the 500hPa height are presented in Fig. 22. These show the T213/L31 forecasts in a less favourable light. This result presumably reflects the larger eddy amplitudes found in the new version of the model.

The mean skill scores computed for the European region show quite substantially better results for T213/L31. This is seen particularly clearly for anomaly correlations, which are presented in Fig. 23, but is found also for standard deviations. Results for such limited areas show much more scatter than for the extratropical hemispheres, making assessment of significance even more difficult. A tendency for an improvement in scores for Europe which is better than average is, however, also a feature of the earlier experimentation with increased horizontal and vertical resolution. Conversely, results from the parallel run are poorer for T213/L31 than for T106/L19 over the North Atlantic, but this behaviour was not seen previously.

Verification of wind forecasts for 200hPa in the tropics is shown in Fig. 24. As for the height field in the extratropics, the correlation score favours T213/L31 and the root-mean-square favours T106/L19. However, despite truncation of fields to T63, the more intense wind fields seen in both the T213/L31 forecasts and in the corresponding analyses tend to bias verification in favour of T106/L19. An example is presented in Fig. 25. The upper panel of this figure is the standard verification in terms of absolute correlations of the 850hPa vector wind for the extratropical northern hemisphere, and shows what was initially regarded as a disturbingly poorer performance by T213/L31 quite early in the forecast range. The lower panel illustrates how the early advantage of T106/L19 disappears when the verification is carried out between T213/L31 forecasts and T106/L19 analyses, and between T106/L19 forecasts and T213/L31 analyses. A similar result is found for the tropical wind verification.

The most dramatic change seen in the objective verification is in the temperature field at 200hPa for the extratropical northern hemisphere. Anomaly correlations and standard deviations are presented in Fig. 26. Examination of sets of test forecasts indicates that both the increase in vertical resolution and the change of parametrization, and possibly also the use of the semi-Lagrangian advection scheme, contribute to this improvement.

Data assimilation statistics also show improved thermal structures near the tropopause with the T213/L31 system. Fits of first-guess and analyzed thicknesses to radiosonde observations are distinctly better than in the operational system at levels around the tropopause (Fig. 27). Here increased vertical resolution removes a component of the bias which changes sign from one 50hPa layer to the next. This arises when analyzed temperature increments have to be calculated at model levels which approximately coincide with the standard

pressure levels at which geopotential is analyzed. This is the case near the tropopause with the 19-level vertical resolution. Away from the tropopause, temperature fits are slightly in favour of T213/L31 for the analyses, but in favour of T106/L19 for the first guesses. This behaviour can be seen at almost all levels in the results for the zonal wind component included in Fig. 27 and arises mainly from bias in the T213/L31 first guess. First-guess statistics for the meridional wind component point to better fits for T213L31 in the troposphere, but again to poorer six-hour wind forecasts in the stratosphere.

Examination has also been made of ensemble-averaged zonal-mean forecast errors at the five-day range. Moisture fields show an increased drying of the lower troposphere for T213/L31, a result consistent with the increased initial imbalance in the global-mean hydrological budget discussed above. T213/L31 shows less of an erroneous drying of the upper troposphere. The principal difference in temperature errors is a marked reduction in the cooling found in the T106/L19 model around 200hPa at middle and high latitudes of the summer hemisphere. Comparison of a set of point soundings for this region shows that the new model also does not exhibit the tendency for a relatively moist lower stratosphere that is seen for T106/L19. Elsewhere, temperature errors are much smaller, but there is a more widespread cooling with T213/L31. An increased radiative cooling more than compensates for the increased latent heating that occurs in the troposphere in the new version of the model. In the stratosphere there is a contribution from the change in numerical scheme, since the semi-Lagrangian version of the model tends to give a cooler upper atmosphere than the Eulerian version. The reason for this is not yet known.

The amount of horizontal diffusion applied at upper model levels is being reconsidered. After completion of the parallel run we became aware of the existence of extremely strong temperature gradients and winds in the polar night vortex of the southern hemisphere. The operational analysis for the last day for which parallel forecasts were carried out showed a wind maximum of 126ms^{-1} at 10hPa, and this rose to a peak of 143ms^{-1} in the operational four-day forecast from this day. With such velocities the Eulerian T106/L19 code invokes a very heavy upper-level damping to ensure computational stability. Such damping had been removed for the semi-Lagrangian version of the model, and whilst the T213/L31 model was stable in this case, noise was evident in the 10 and 30hPa divergent wind components along the jet axis for a short period around day 4. More generally, the divergence field near the top of the high-resolution model reflects the presence of the underlying orography, presumably through vertically propagating gravity waves. Whatever their realism elsewhere, these waves are not accurately represented close to the model top. It appears that the increased horizontal diffusion employed in the stratosphere to damp these waves is insufficient for its intended purpose.

6. CONCLUSIONS

Changes in model formulation have been successfully developed to make possible the operational use of a T213/L31 version of the ECMWF spectral model on the CRAY Y-MP8 computer. Very few problems in the area of model performance were encountered in implementation of the reduced Gaussian grid. This was a substantial technical exercise, but one which has been carried out in such a way as to cause minimal consequences for the majority of users of the model.

The semi-Lagrangian method for the representation of advection has been shown to be feasible for medium-range weather prediction. A six-fold increase in timestep has been achieved at T213/L31 resolution, and the extra computational cost of the scheme has been kept within a reasonable bound. A major reorganization of the model was required, and this contributed towards enabling a significant increase in the efficiency of the Legendre transforms.

In development of the semi-Lagrangian formulation, several choices had to be made with respect to the choice of prognostic variables, the evaluation of right-hand side terms in the governing equations, the formulation of the continuity equation and the implementation of the semi-implicit treatment of gravity-wave terms. Although a working scheme has been produced, improvements are possible, and further attention will be devoted to these topics. The principal assessment of the scheme has been at T106/L31 and T213/L31 resolutions, and future work will also include examination of the performance of the scheme at the lower resolutions currently used to establish the model climatology and for trials of Monte Carlo forecasting.

Two more substantial lines of development will also be pursued. The first is the representation of the humidity field as a grid-point rather than spectral variable, using a shape-preserving interpolation method following the work of *Rasch and Williamson* (1990). Encouraging results have been obtained from initial tests of this approach, which should also be appropriate for the advection of any additional prognostic fields that are included in the model. The other topic of development will be investigation of a two-time-level formulation of the model, which offers the possibility of a further reduction in computational time and memory requirements.

The increase in resolution to T213/L31 brings about a distinct improvement in forecasts for lower atmospheric levels out to about four days in most test forecasts carried out from analyses produced using the T106/L19 system. Results show the expected local improvement in predicted weather elements, and there is an increase in the intensity and realism of synoptic-scale systems. The latter is beneficial to the quality of forecasts over the first half of the ten-day range, but can bias objective verification scores against the higher resolution once the overall forecast accuracy has deteriorated significantly. Evidence of the more active nature of the new

version of the model is seen in significant increases in global-mean precipitation and eddy kinetic energy. The increases arise both from the changed horizontal and vertical resolution, and from the accompanying change in the parametrization of clouds and radiation.

It is premature to draw too firm conclusions as to the overall impact of the model change, including data assimilation, on the basis of what is, at the time of writing, an incompletely diagnosed parallel run of limited duration from a high-summer month. Some promising synoptic improvements have been found, and there is an indication of a more positive impact on some objective scores than found when running from interpolated T106/L19 analyses. The European region appears especially to benefit from use of the new model version. It is perhaps not surprising that with a model change of this order improvements are not seen in all aspects of model behaviour. The over-prediction of rainfall in the early stages of the model runs, which occurs repeatedly in the short-range forecasts of the data assimilation, is a cause for particular concern. Nevertheless, with its more realistic eddy energy and capability for better description of topographic effects and frontal, boundary-layer and tropopause structures, the new model version has the potential for important future contributions to the improvement of the Centre's forecasts.

References

Hortal, M. and A.J. Simmons, 1991: Use of reduced Gaussian grids in spectral models. Mon.Wea. Rev., 119, 1057-1074.

Janssen P.A.E.M., A.C.M. Beljaars, A.J. Simmons and P. Viterbo, 1991: On the determination of surface stress in an atmospheric model. In preparation.

Machenhauer, B., 1979: The spectral method. GARP Publication Series No. 17, Vol. 2, WMO, Geneva, 121-175.

Rasch, P.J., and D.L. Williamson, 1990: Computational aspects of moisture transport in global models of the atmosphere. Q.J.R.Met.Soc., 116, 1071-1090.

Ritchie, H., 1987: Semi-Lagrangian advection on a Gaussian grid. Mon.Wea.Rev., 115, 608-619.

Ritchie, H., 1988: Application of the semi-Lagrangian method to a spectral model of the shallow water equations. Mon.Wea.Rev., 116, 1587-1598.

Ritchie, H., 1991: Application of the semi-Lagrangian method to a multilevel spectral primitive-equations model. Q.J.R.Met.Soc., 117, 91-106.

Robert, A., 1981: A stable numerical integration scheme for the primitive meteorological equations. Atmos.Ocean, 19, 35-46.

Simmons, A.J. and D. Dent, 1989: The ECMWF multi-tasking weather prediction model. Computer Physics Reports., 11, 165-194.

Simmons, A.J., L. Dell'Osso, M. Jarraud, J.-M. Hoyer and G. Sakellarides, 1987: Some results from studies of increased horizontal and vertical resolution. ECMWF Technical Memorandum No. 136, 52pp.

Simmons, A.J., D.M. Burridge, M. Jarraud, C. Girard and W. Wergen, 1989: The ECMWF medium-range prediction models. Development of the numerical formulations and the impact of increased resolution. Met.Atmos.Phys., 40, 28-60.

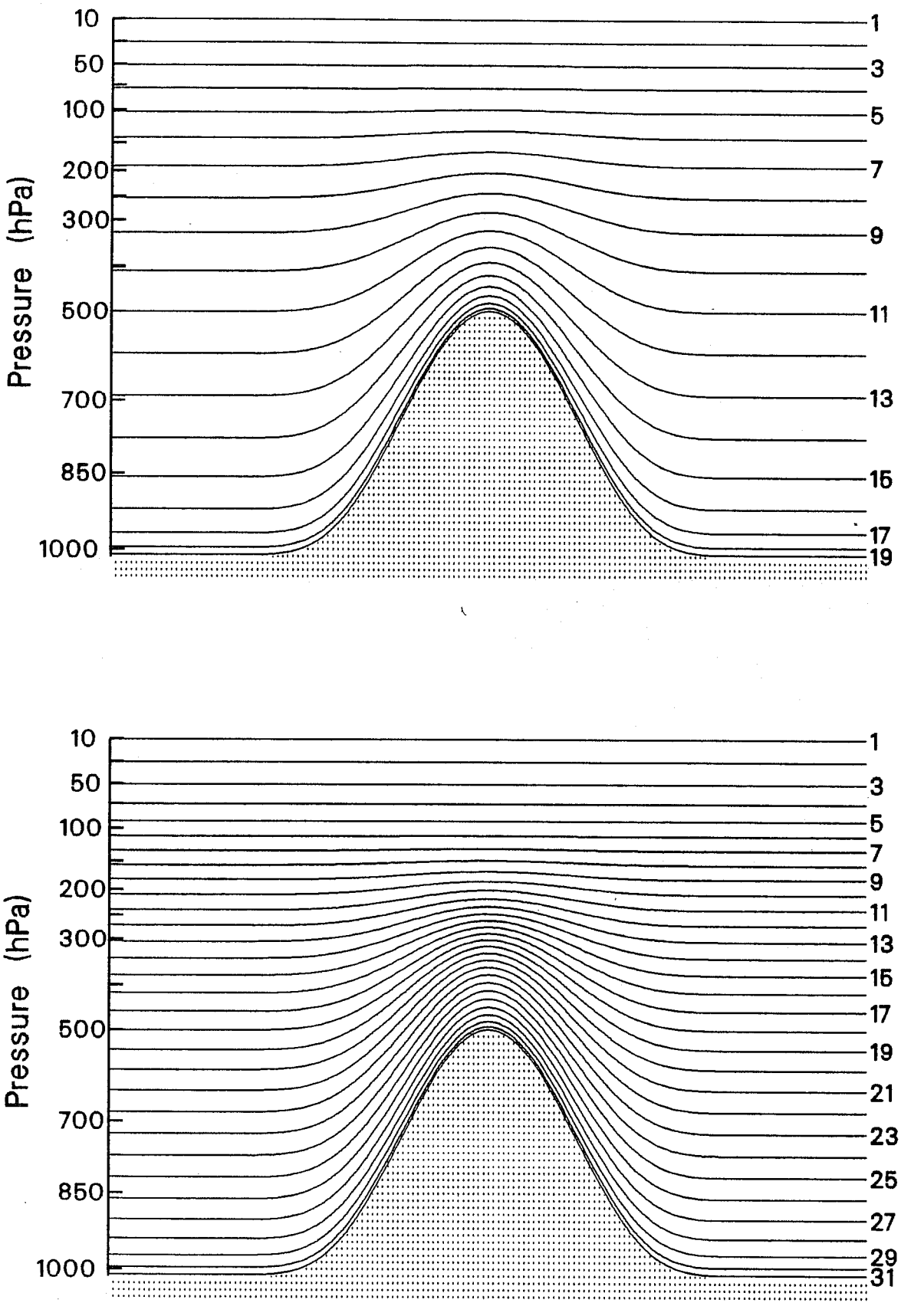

Fig. 1 The 19- and 31-level vertical resolutions.

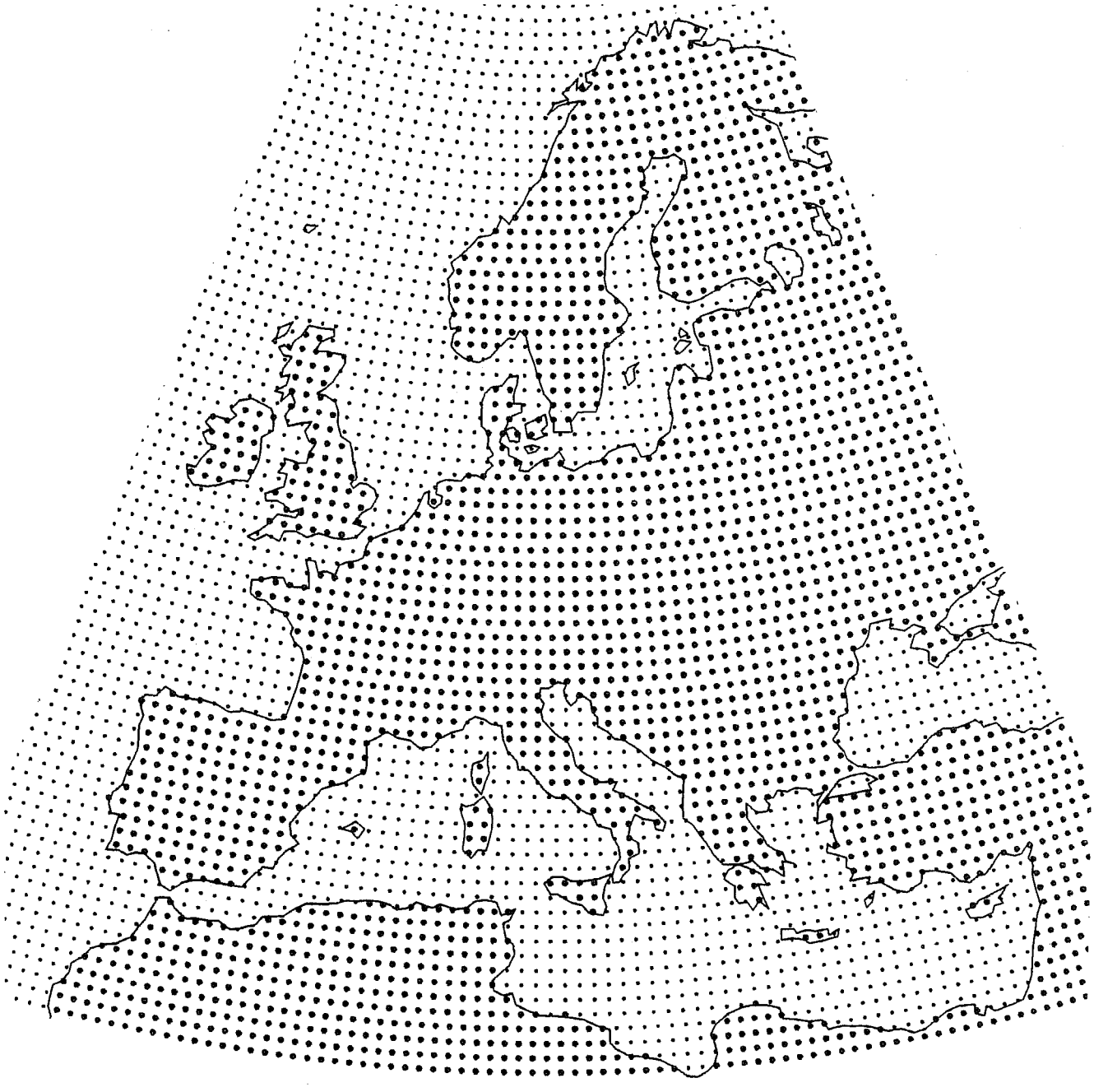

Fig. 2 The reduced grid over Europe for T213 resolution. Heavier dots indicate grid-points treated as land in the model, and lighter dots indicate sea points.

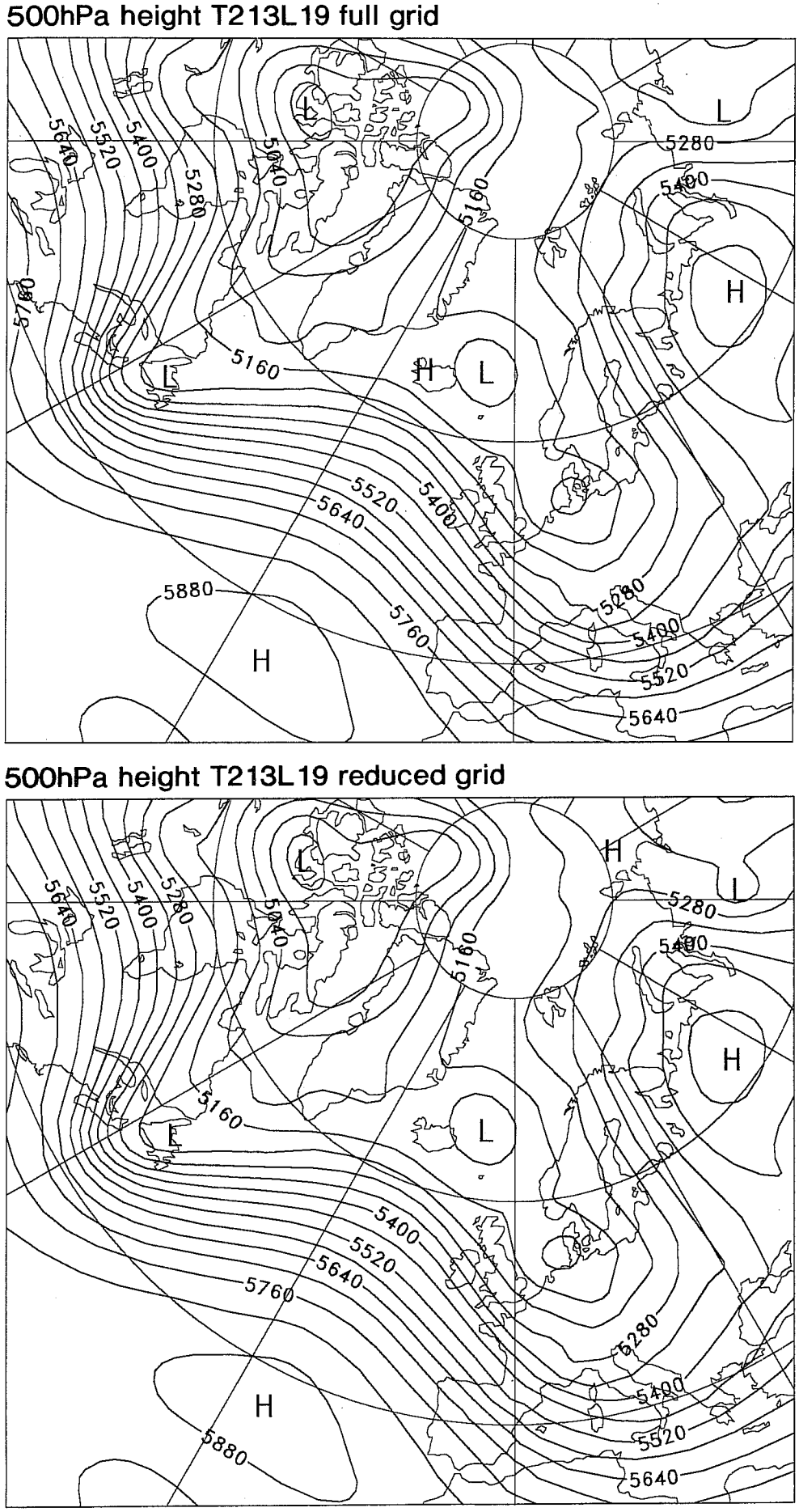

Fig. 3 Day-5 forecasts of 500hPa height from 12UTC 20 March 1986 at T213/L19 resolution using the full grid (upper) and the reduced grid (lower). The contour interval is 60m.

Precipitation T213L19 Full grid
Initial date: 86032012 Range: 96 to 120h

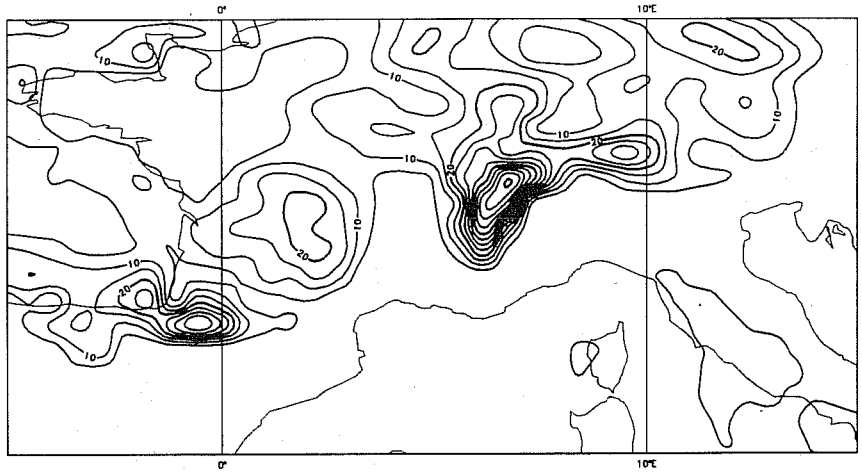

Precipitation T213L19 Reduced grid
Initial date: 86032012 Range: 96 to 120h

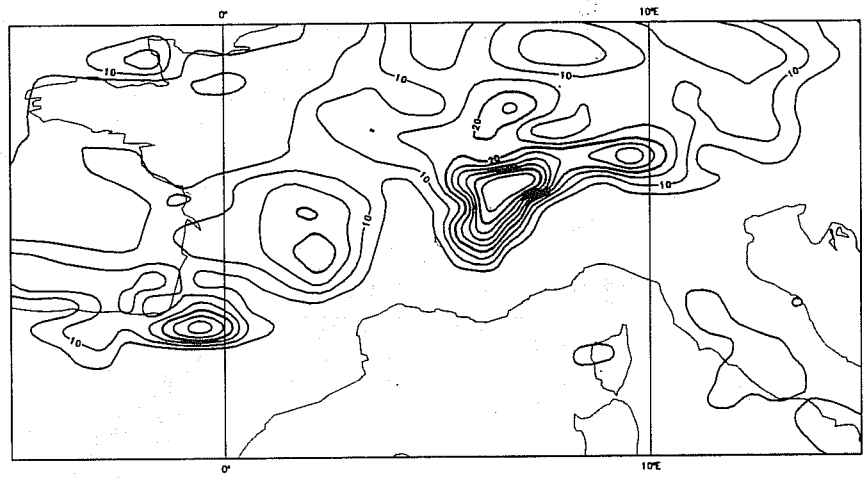

Precipitation T106L19
Initial date: 86032012 Range: 96 to 120h

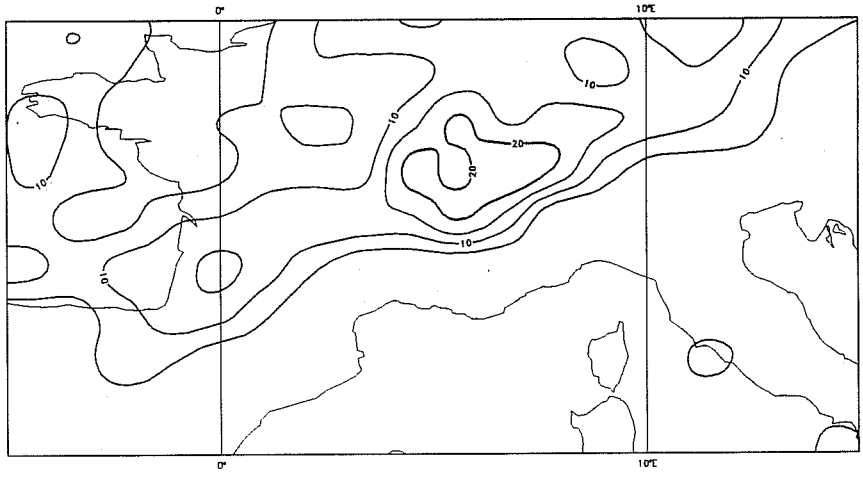

Fig. 4 Precipitation between days 4 and 5 from forecasts from 12UTC 20 March 1986 for:
Upper: T213/L19, full grid.
Middle: T213/L19, reduced grid.
Lower: T106/L19, full grid.
The contour interval is 5mm.

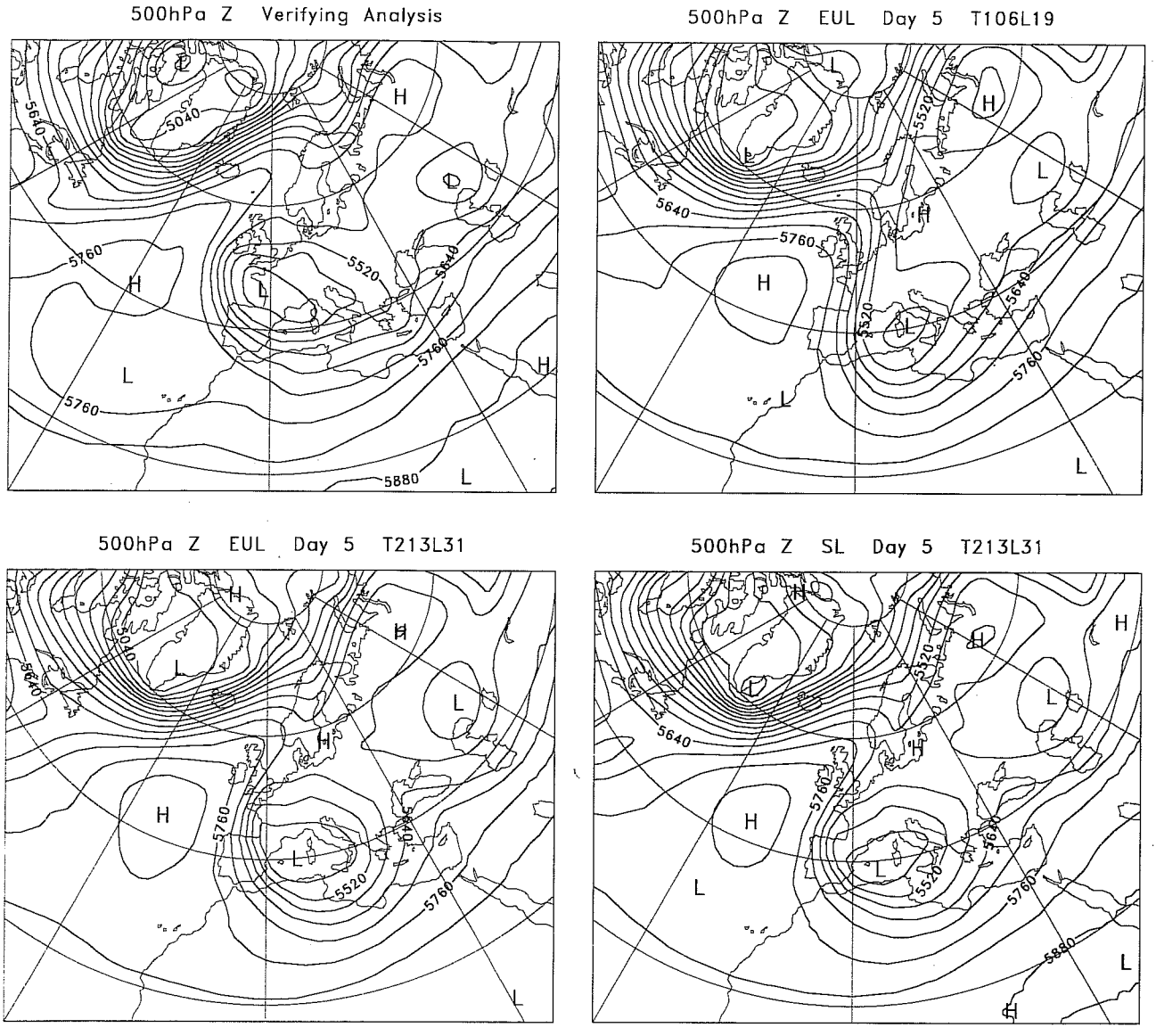

Fig. 5 The analyzed 500hPa height (upper left, contour interval 60m) for 20 April 1990, and day-5 forecasts verifying at this time for:

Upper right: T106/L19, Eulerian, Δt =15min.

Lower left: T213/L31, Eulerian, Δt =3min.

Lower right: T213/L31, Semi-Lagrangian, Δt =20min.

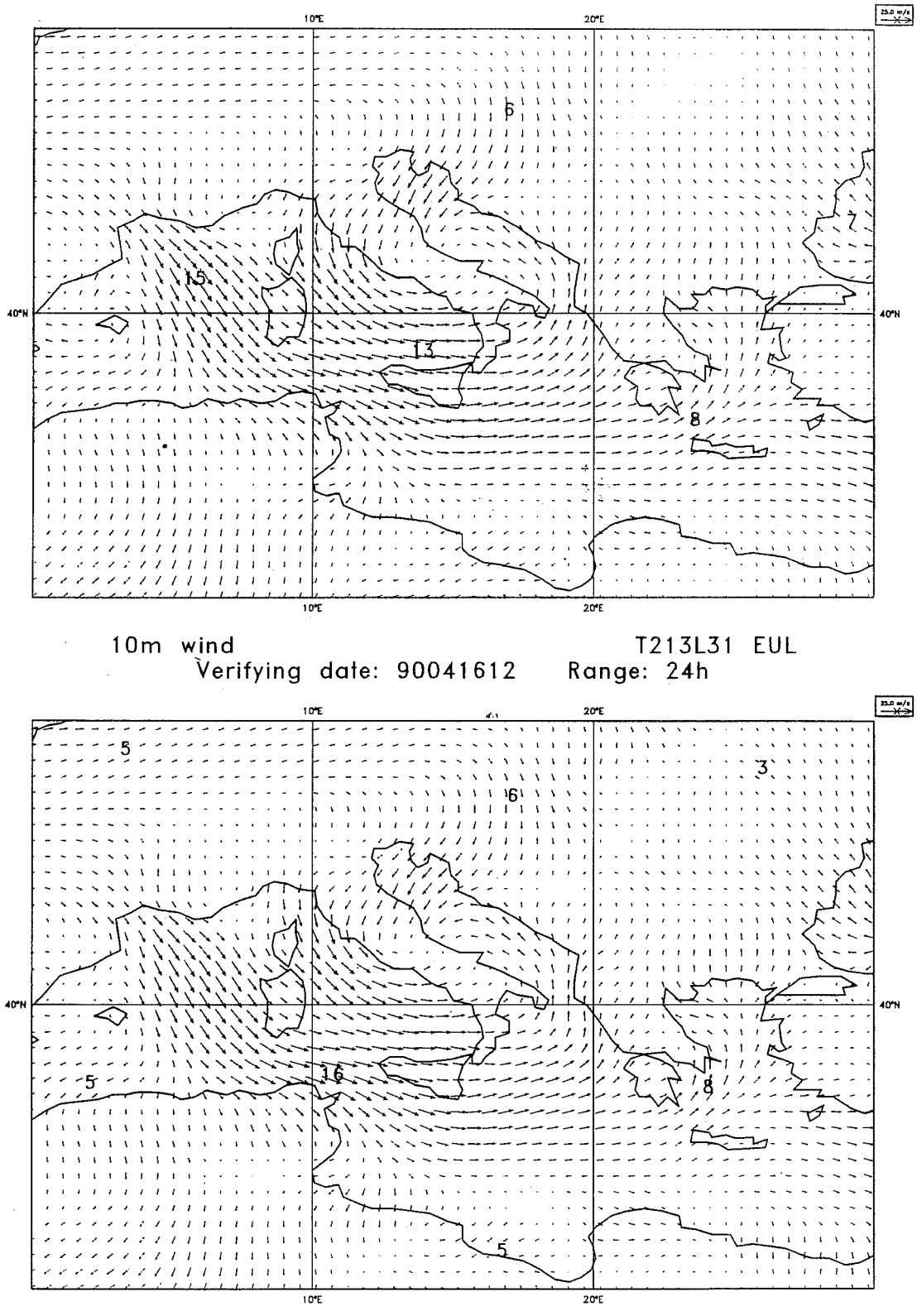

Fig. 6 24-hour forecasts of 10m wind (ms^{-1}) from 15 April 1990, for:
Upper: T213/L31, Semi-Lagrangian, Δt =20min.
Lower: T213/L31, Eulerian, Δt =3min.

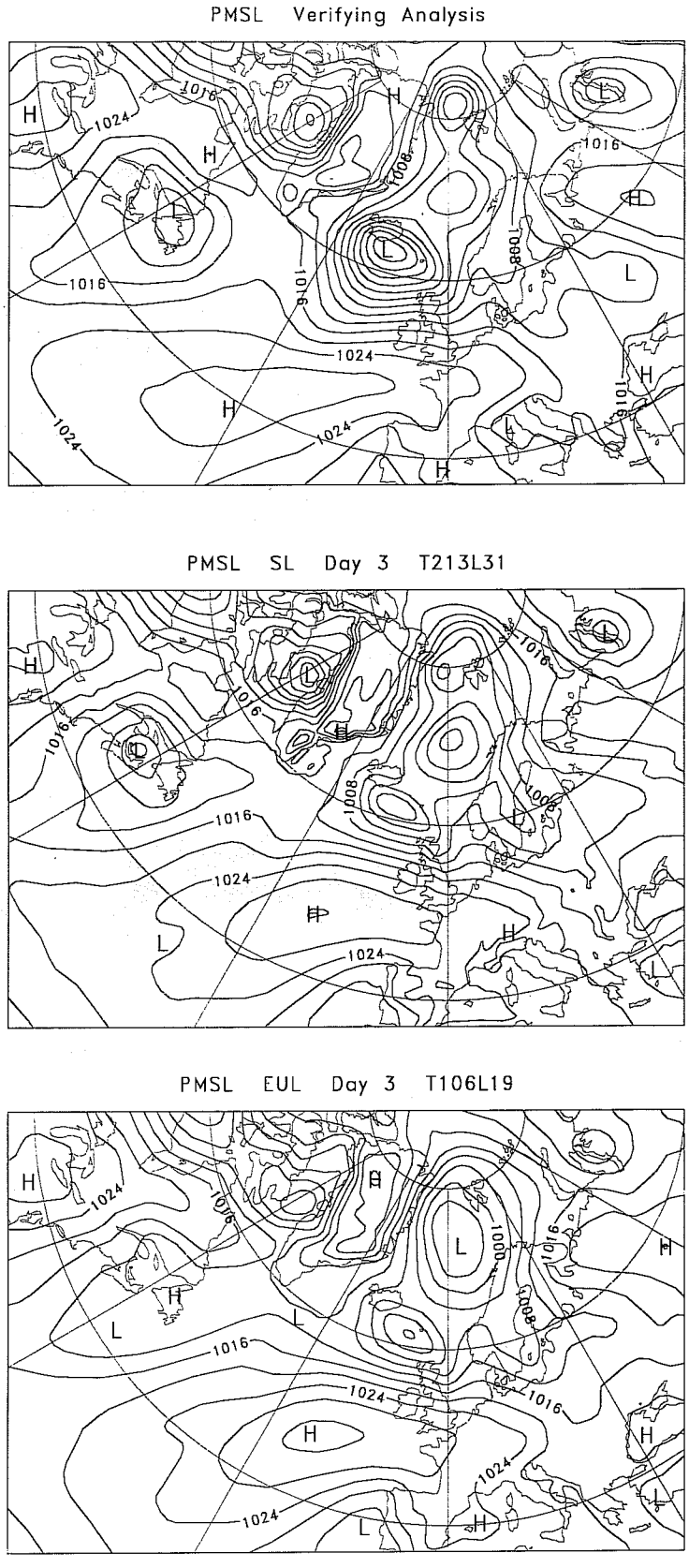

Fig. 7 The analyzed mean sea-level pressure (upper, contour interval 4hPa) for 12UTC 18 September 1990, and day-3 forecasts verifying at this time for T213/L31 (middle) and T106/L19 (lower).

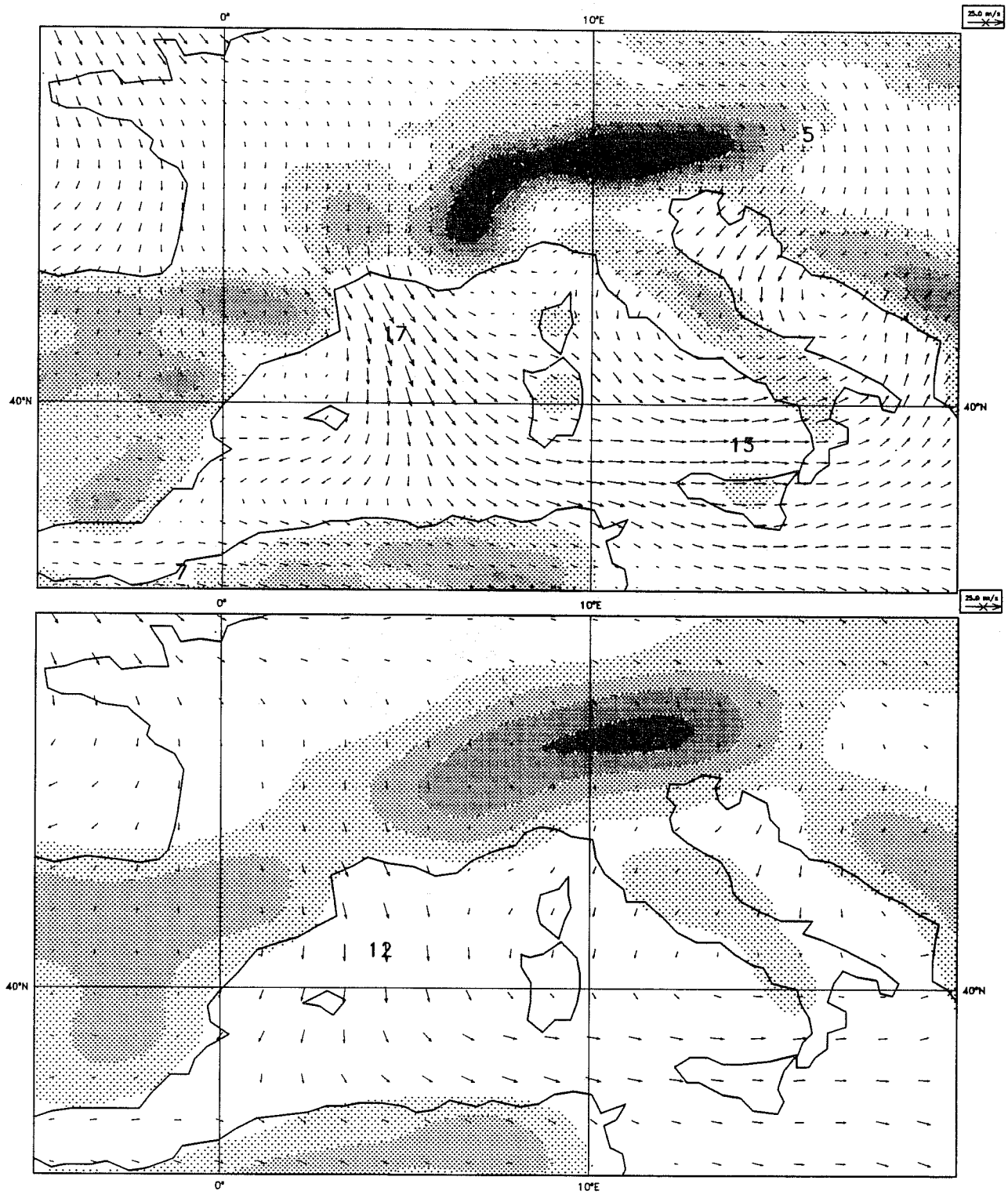

Fig. 8 Day-3 forecasts of 10m wind (ms^{-1}) from 12UTC 15 April 1991 for T213/L31 (upper) and T106/L19 (lower). Model orographies are indicated by shading.

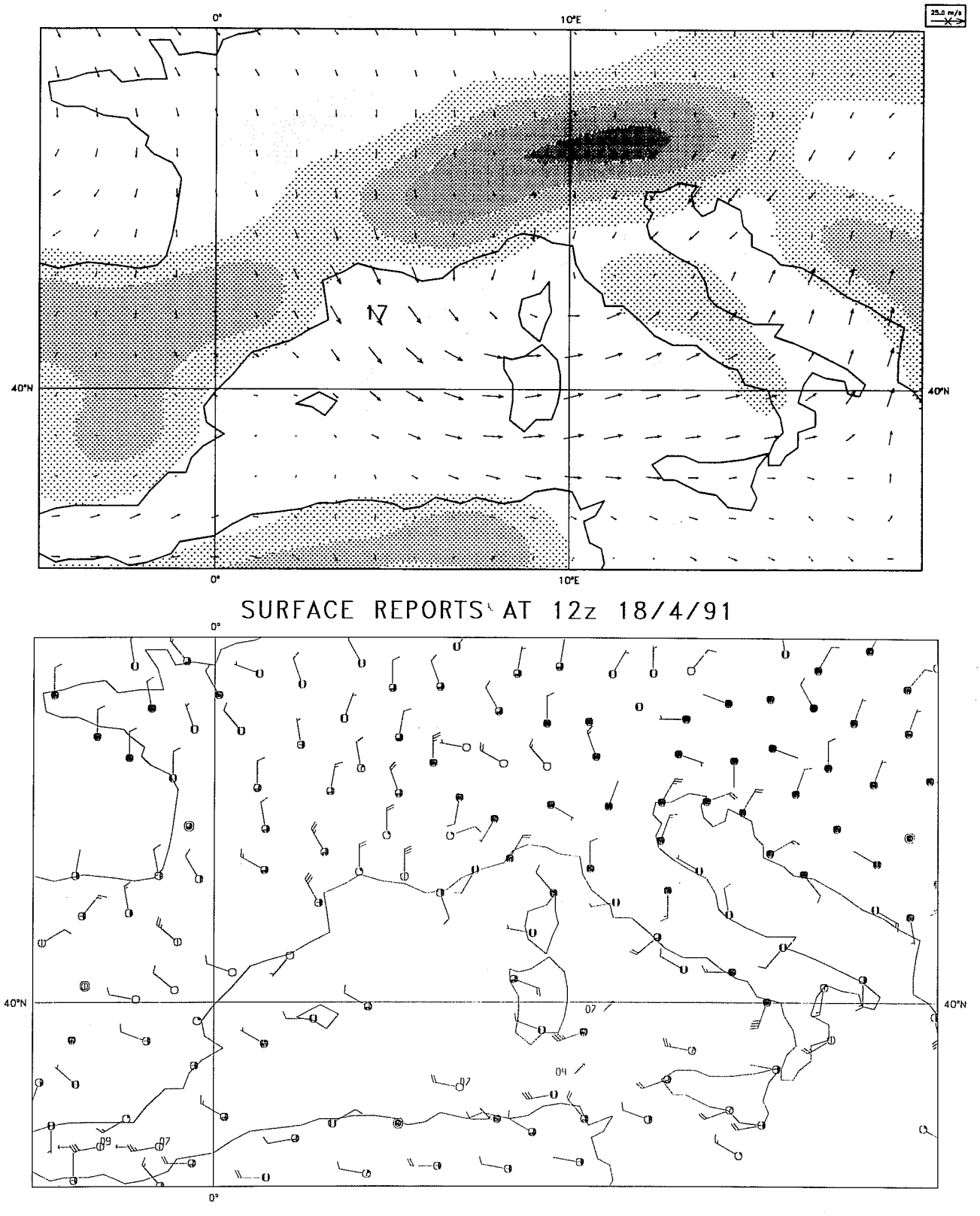

Fig. 9 The verifying (T106/L19) analysis of 10m wind for 12UTC 18 April 1991 (upper), and observed winds (lower).

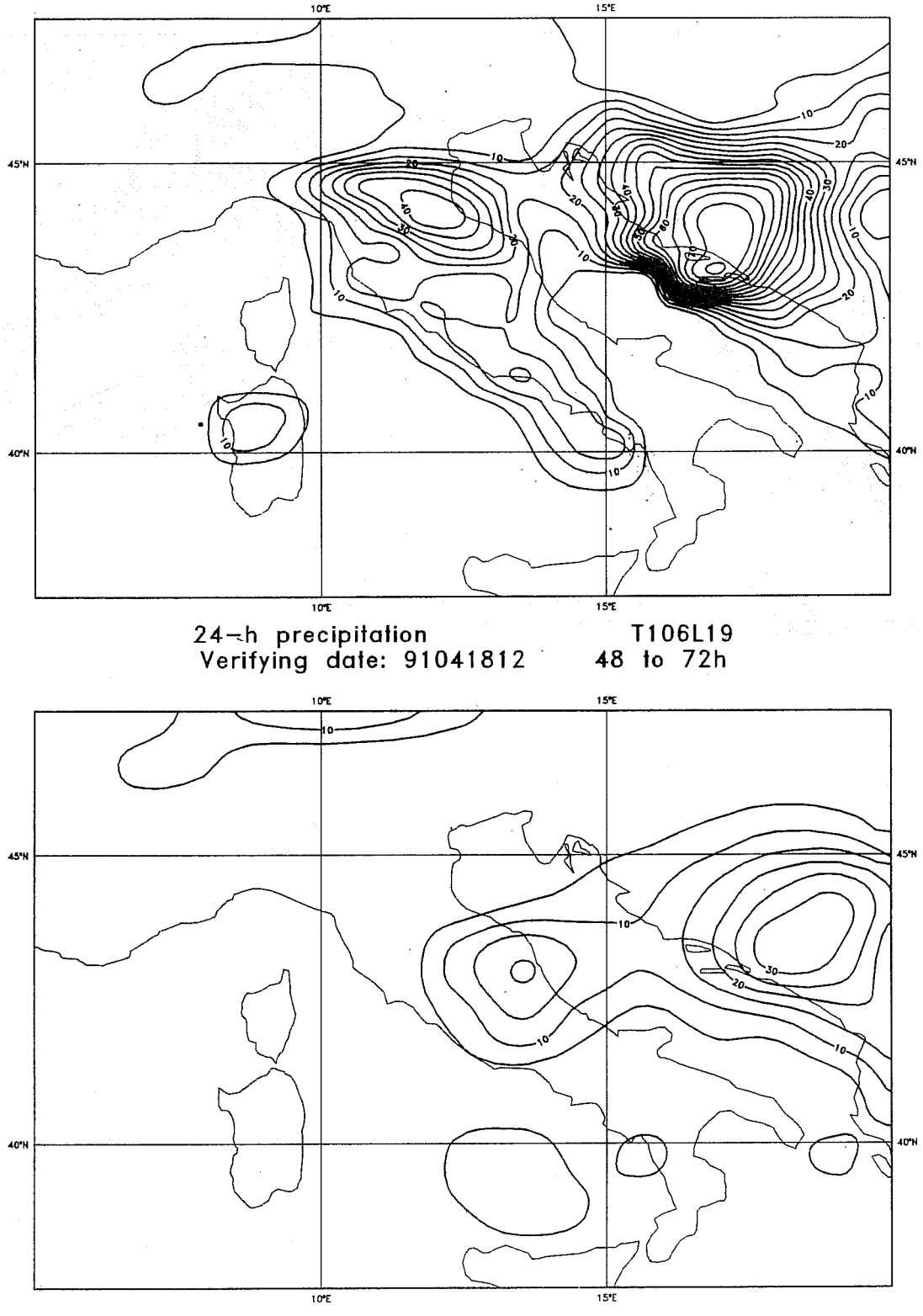

Fig. 10 Forecasts of precipitation (mm) between days 2 and 3 for forecasts from 12UTC 15 April 1991 for T213/L31 (upper) and T106/L19 (lower).

Wednesday 17 April 1991 12Z to Thursday 18 April 1991 12Z
Observed Precipitation

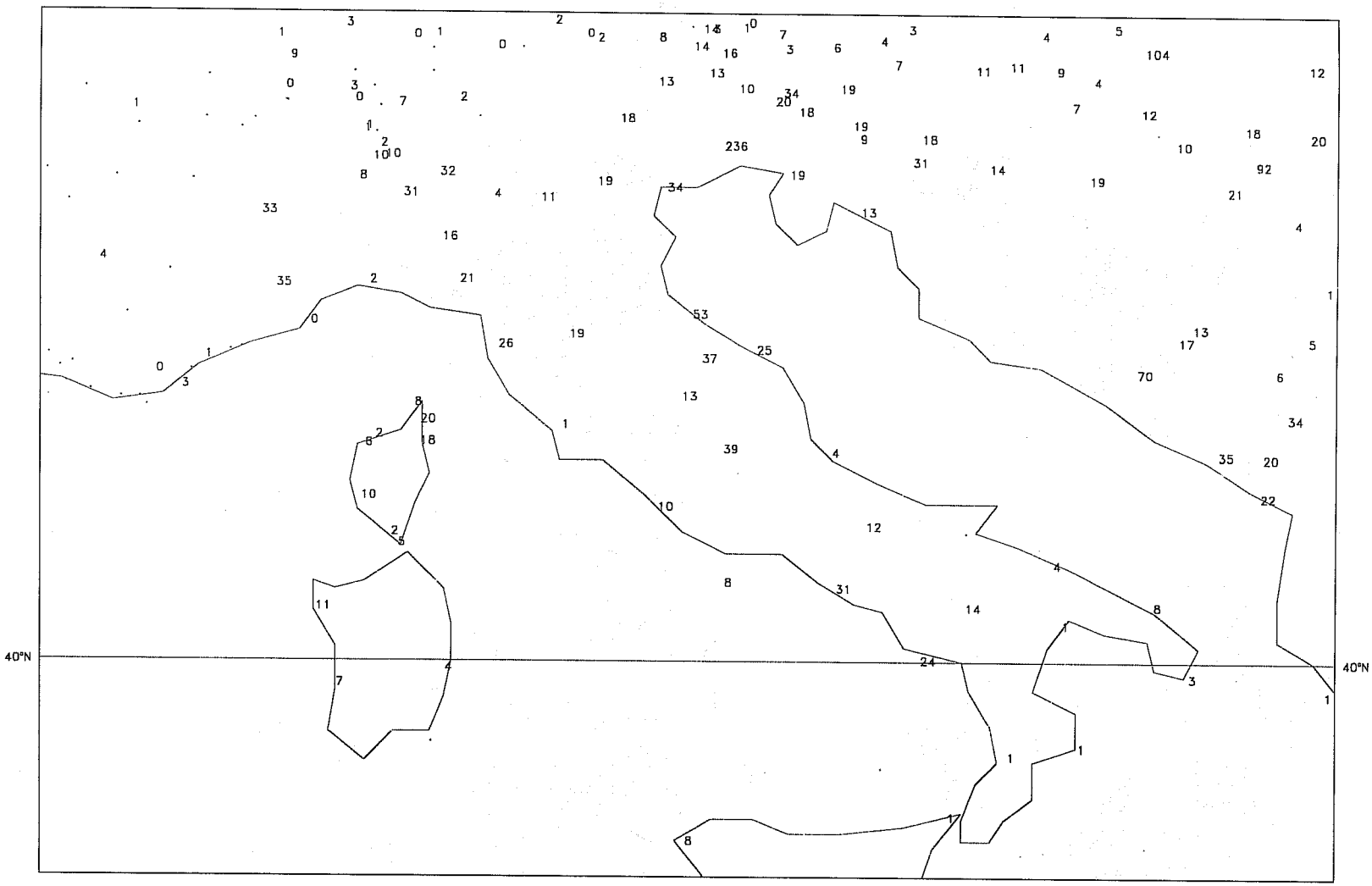

Fig. 11 Observed precipitation (mm) for the period from 12UTC 17 April to 12UTC 18 April 1991.

Day 5

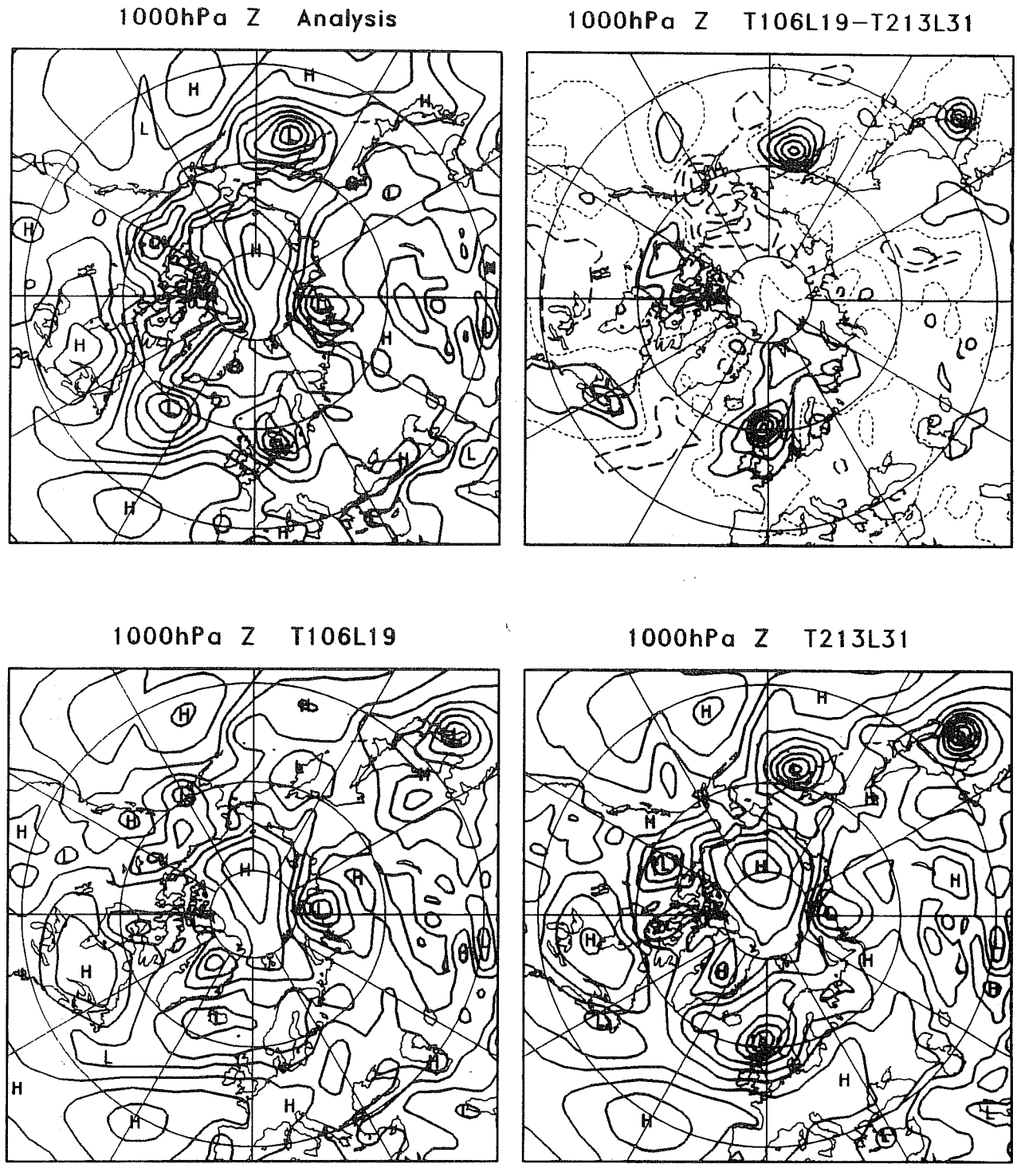

Fig. 12 The analyzed 1000hPa height (upper left, contour interval 40m) for 20 August 1990, and day-5 forecasts verifying at this time for T106/L19 (lower left) and T213/L31 (lower right). The difference between the two forecasts (contour interval 30m) is shown in the upper right panel.

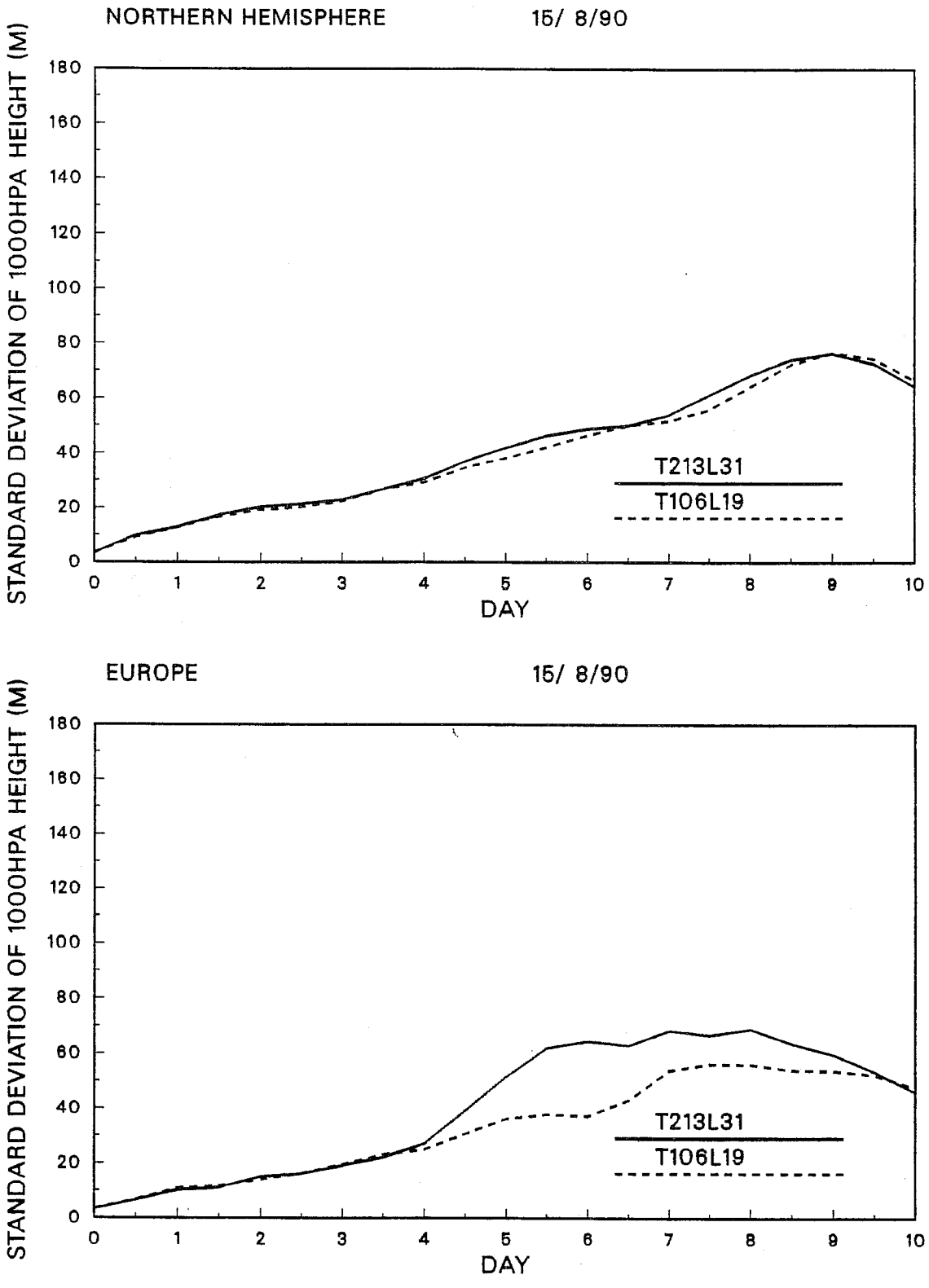

Fig. 13 Standard deviations of 1000hPa height (m) for T213/L31 (solid) and T106/L19 (dashed) for the extratropical northern hemisphere (upper), and for the European region (lower).

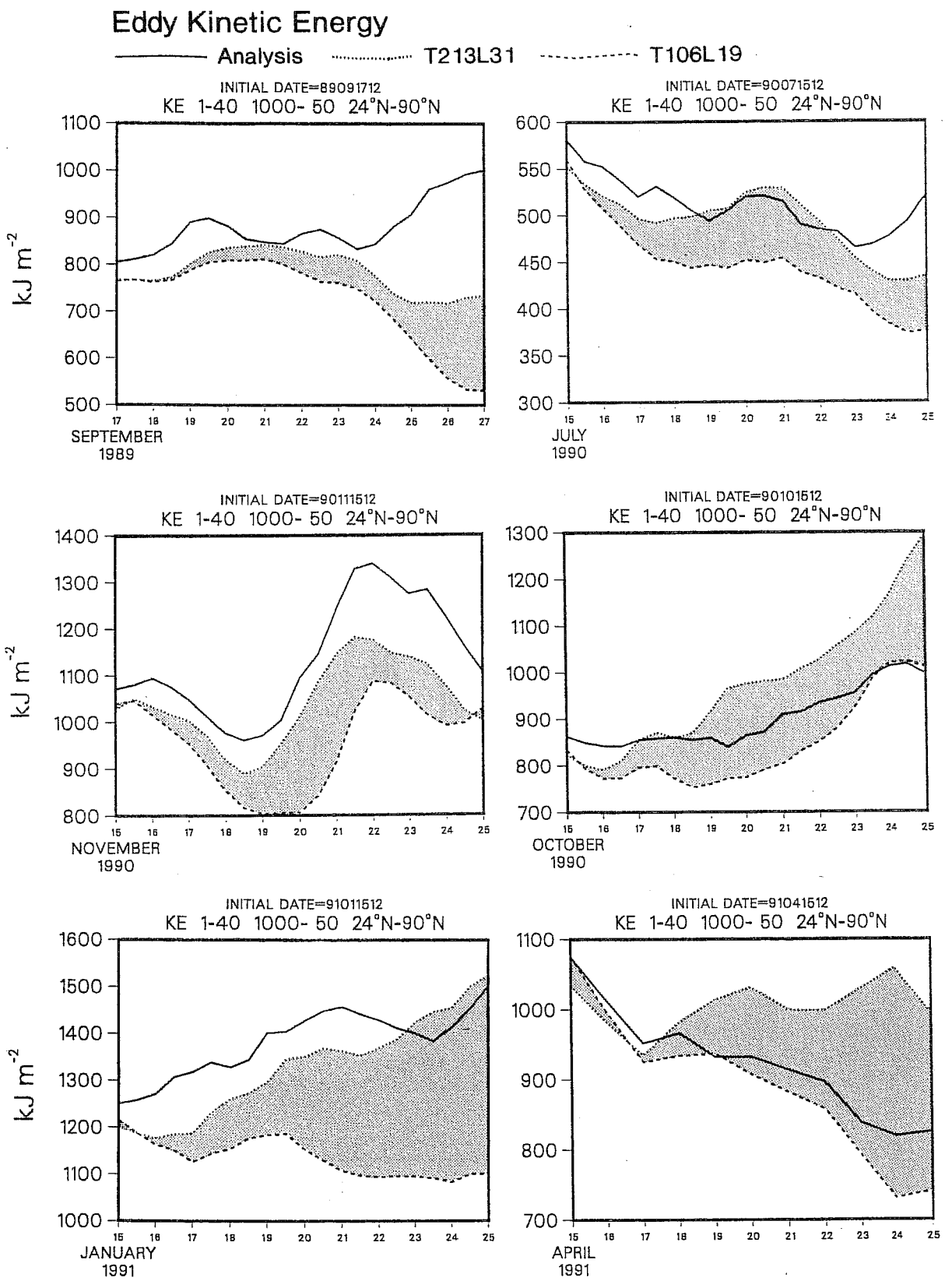

Fig. 14 Eddy kinetic energies for the extratropical northern hemisphere as a function of forecast range for six cases. The solid line denotes the verifying analysis, the dotted line the T213/L31 forecast, and the dashed line the T106/L19 forecast.

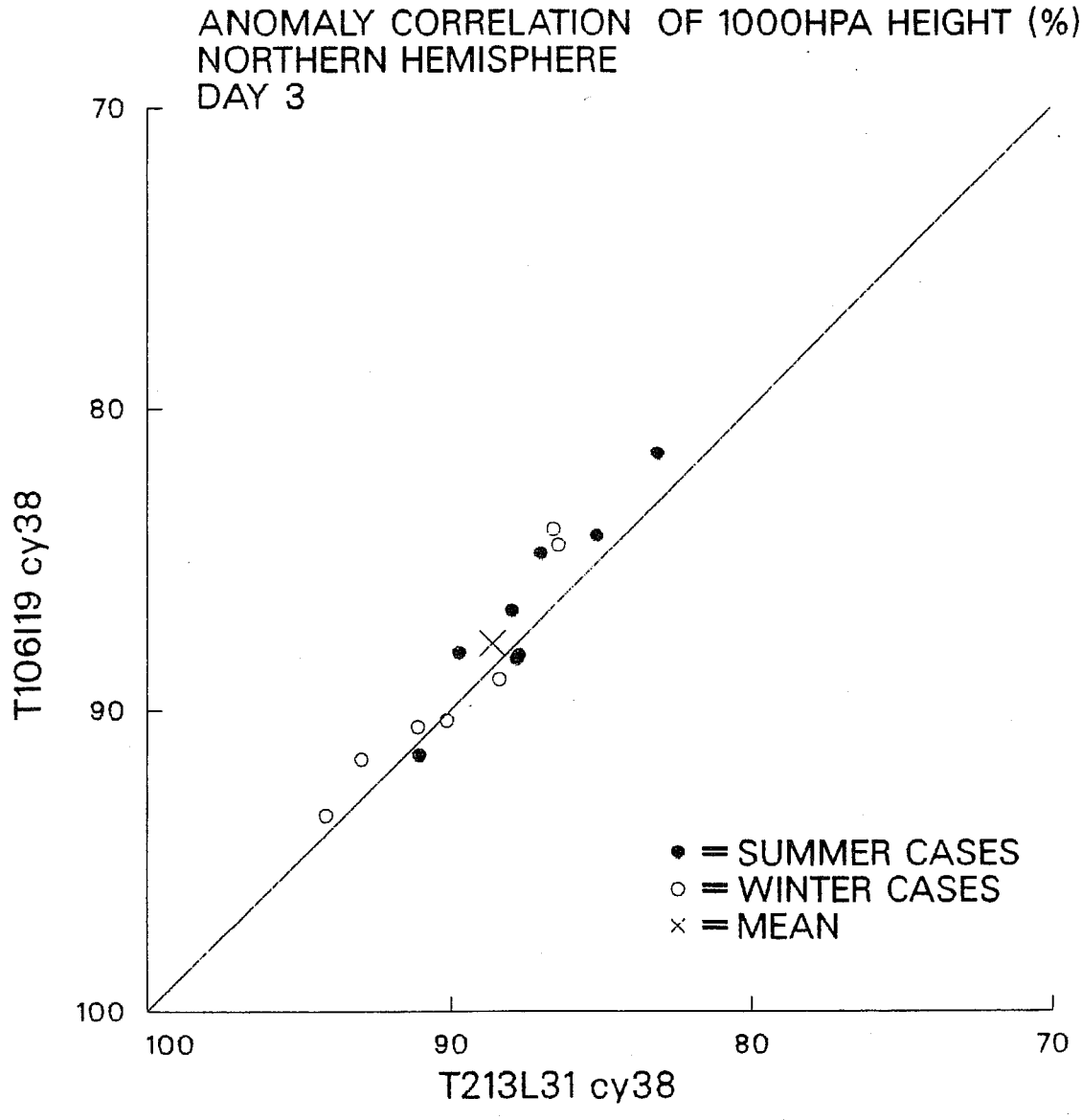

Fig. 15 Anomaly correlations of 1000hPa height (%) for day-3 T213/L31 and T106/L19 forecasts for the extratropical northern hemisphere.

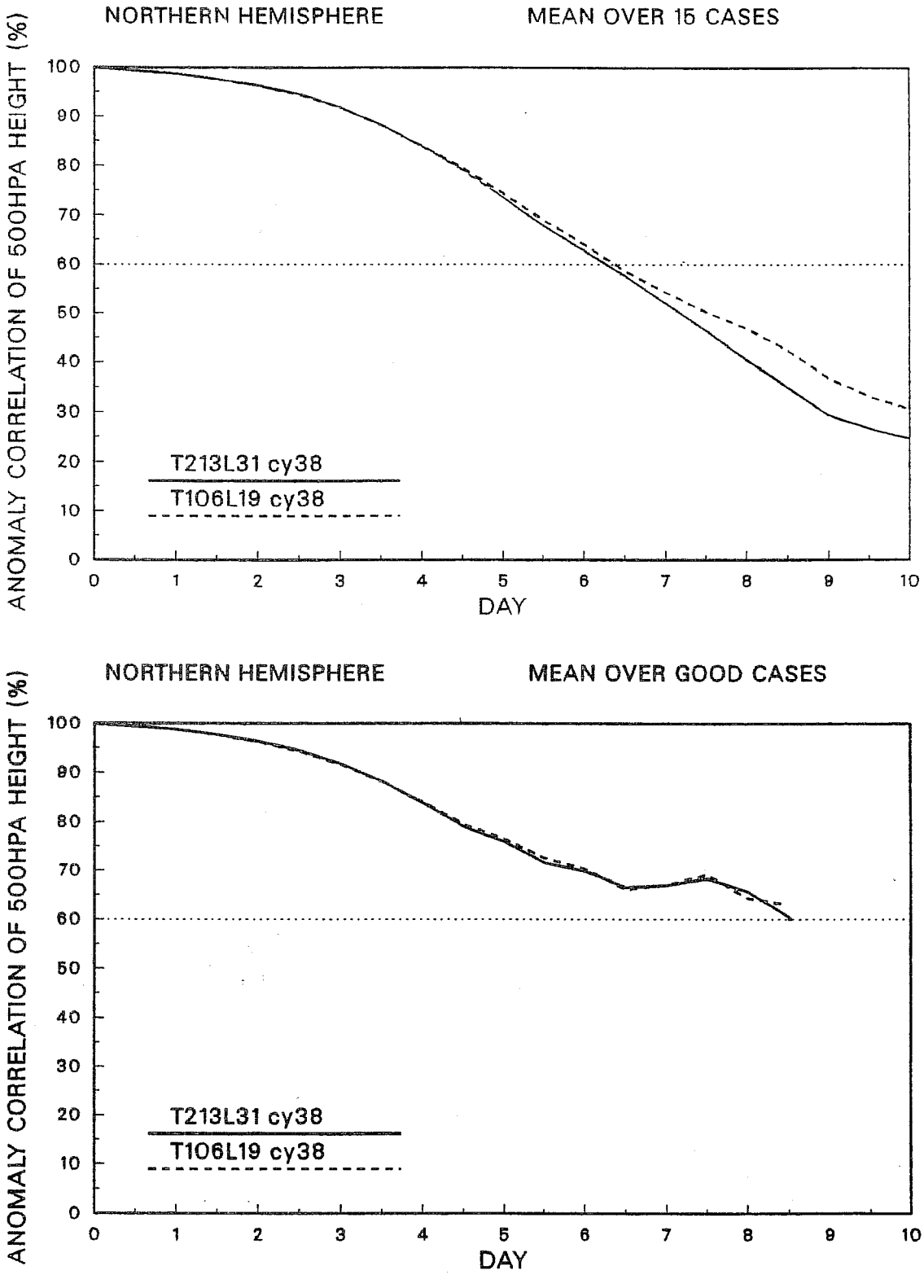

Fig. 16 Mean anomaly correlations of 500hPa height for T213/L31 (solid) and T106/L19 (dashed). In the upper panel the mean is computed over all 15 cases available, and in the lower panel the mean is restricted to cases for which correlations are above 60% for both forecasts.

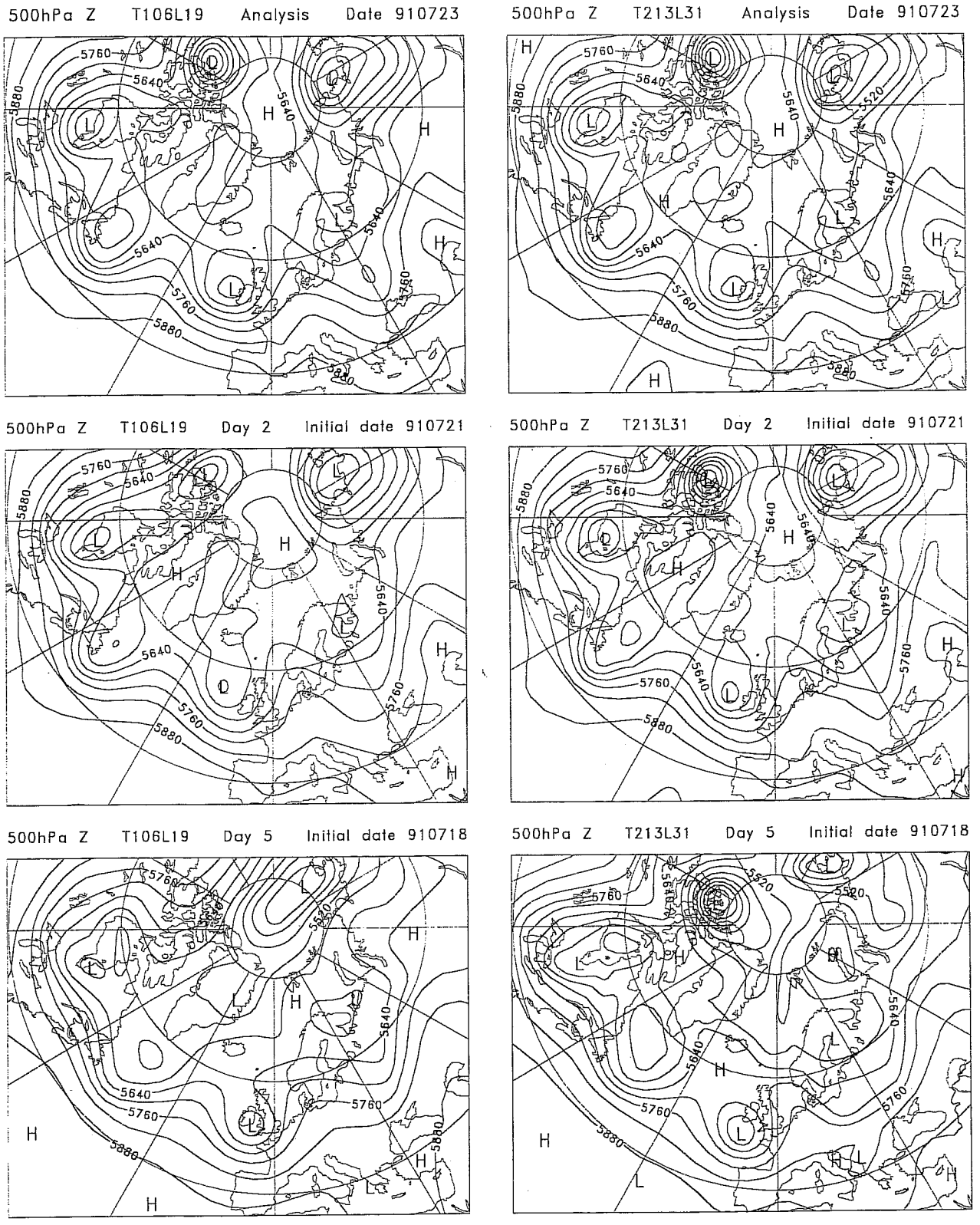

Fig. 17 500hPa analyses (upper, contour interval 60m) for 12UTC 23 July 1991 from T106/L19 (left) and T213/L31(right), and corresponding verifying day-2 (middle) and day-5 (lower) forecasts.

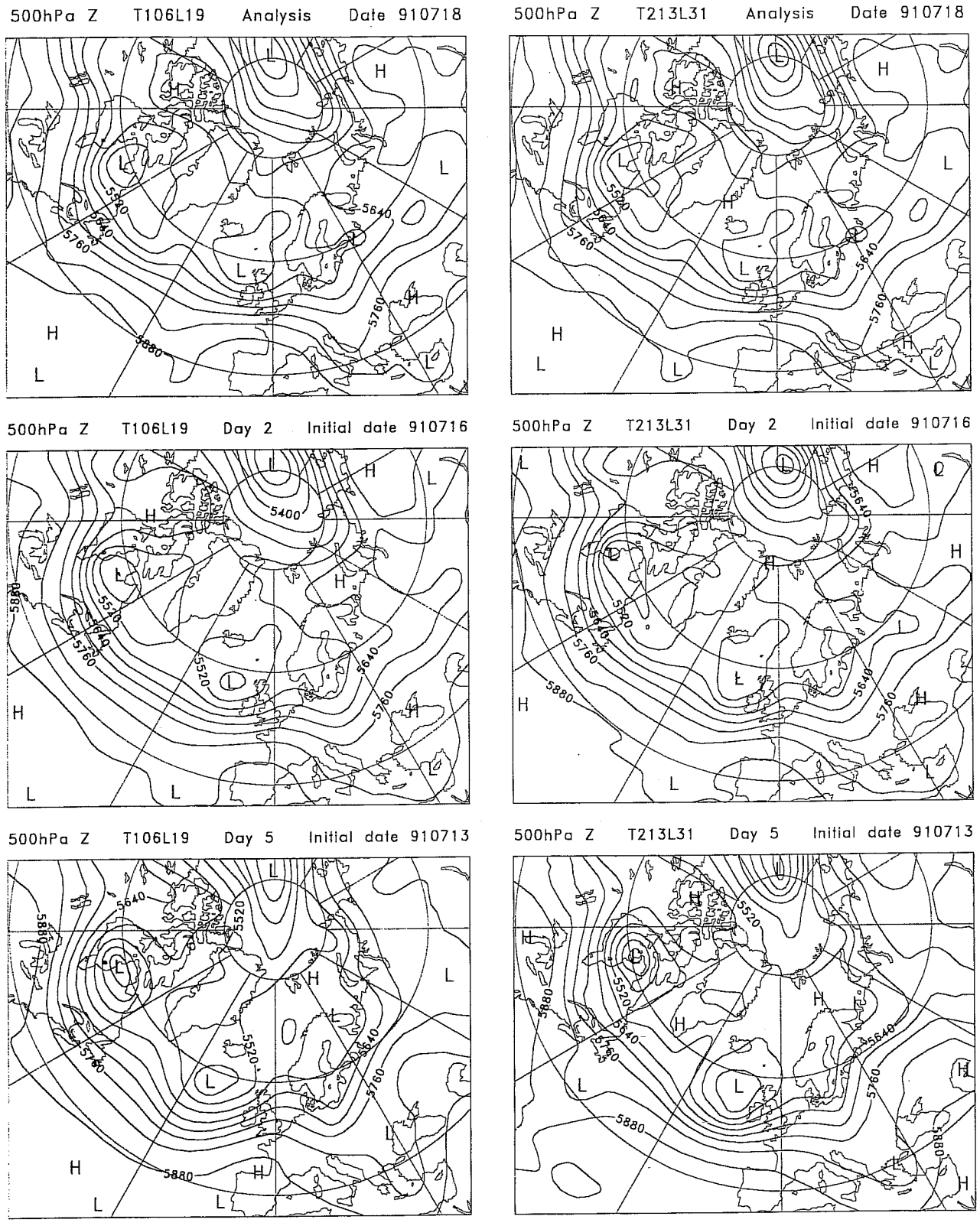

Fig. 18 500hPa analyses (upper, contour interval 60m) for 12UTC 18 July 1991 from T106/L19 (left) and T213/L31(right), and corresponding verifying day-2 (middle) and day-5 (lower) forecasts.

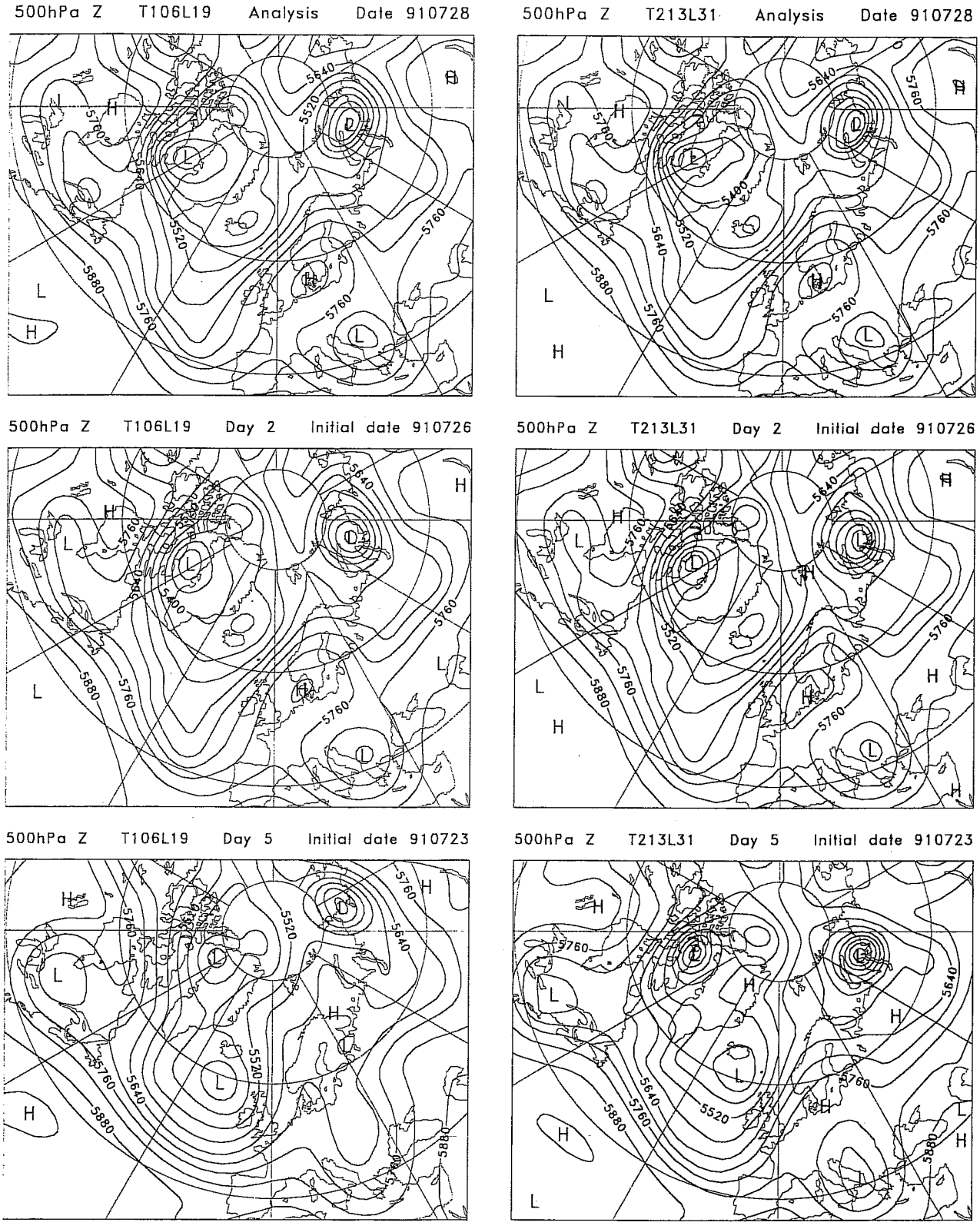

Fig. 19 500hPa analyses (upper, contour interval 60m) for 12UTC 28 July 1991 from T106/L19 (left) and T213/L31(right), and corresponding verifying day-2 (middle) and day-5 (lower) forecasts.

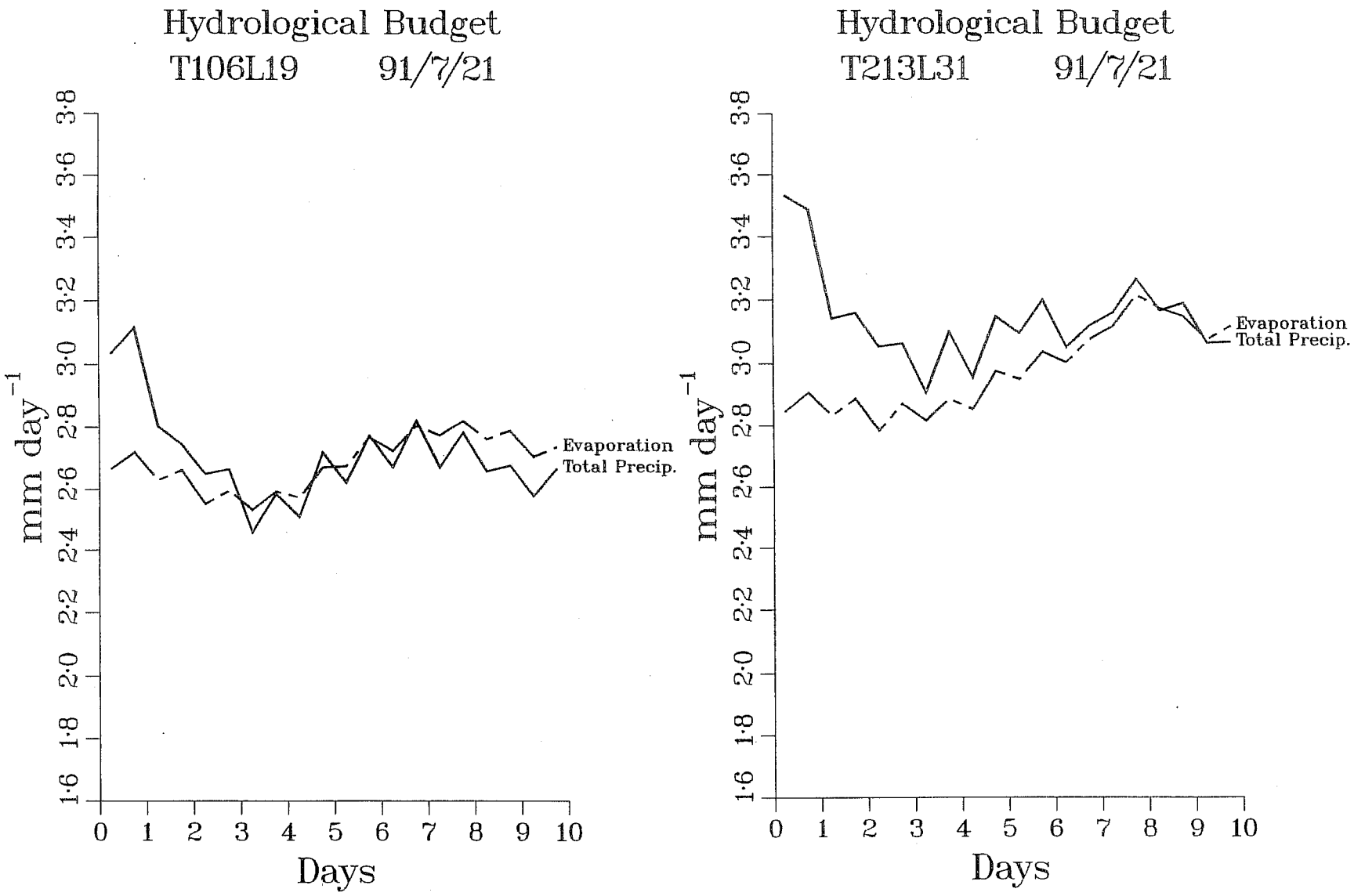

Fig. 20 Global-mean hydrological budgets for T106/L19 (left) and T213/L31 (right) forecasts from 12UTC 21 July 1991.

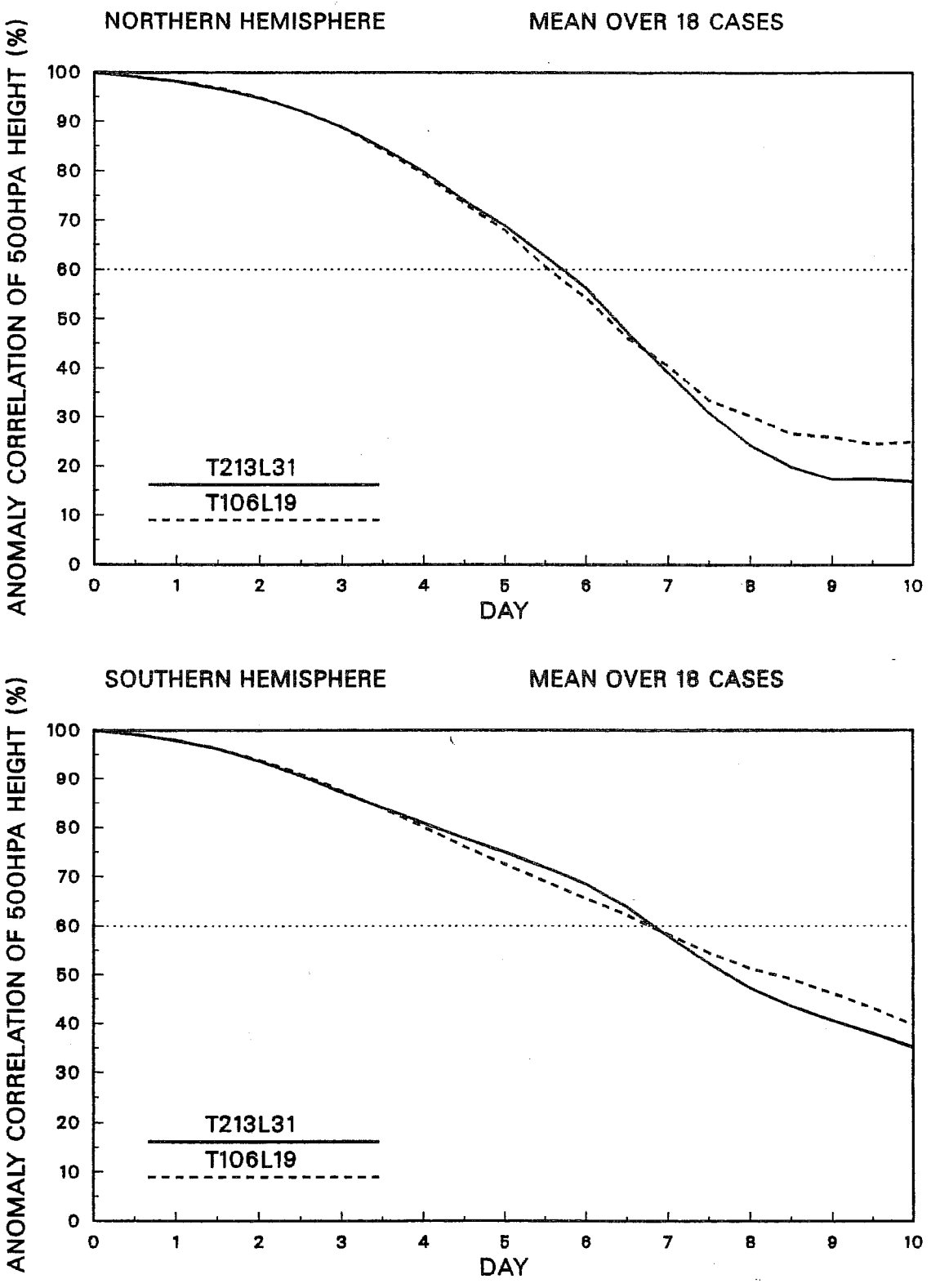

Fig. 21 Mean anomaly correlations of 500hPa height for T213/L31 (solid) and T106/L19 (dashed) for the extratropical northern (upper) and southern (lower) hemispheres, from daily forecasts for the period 11-28 July 1991.

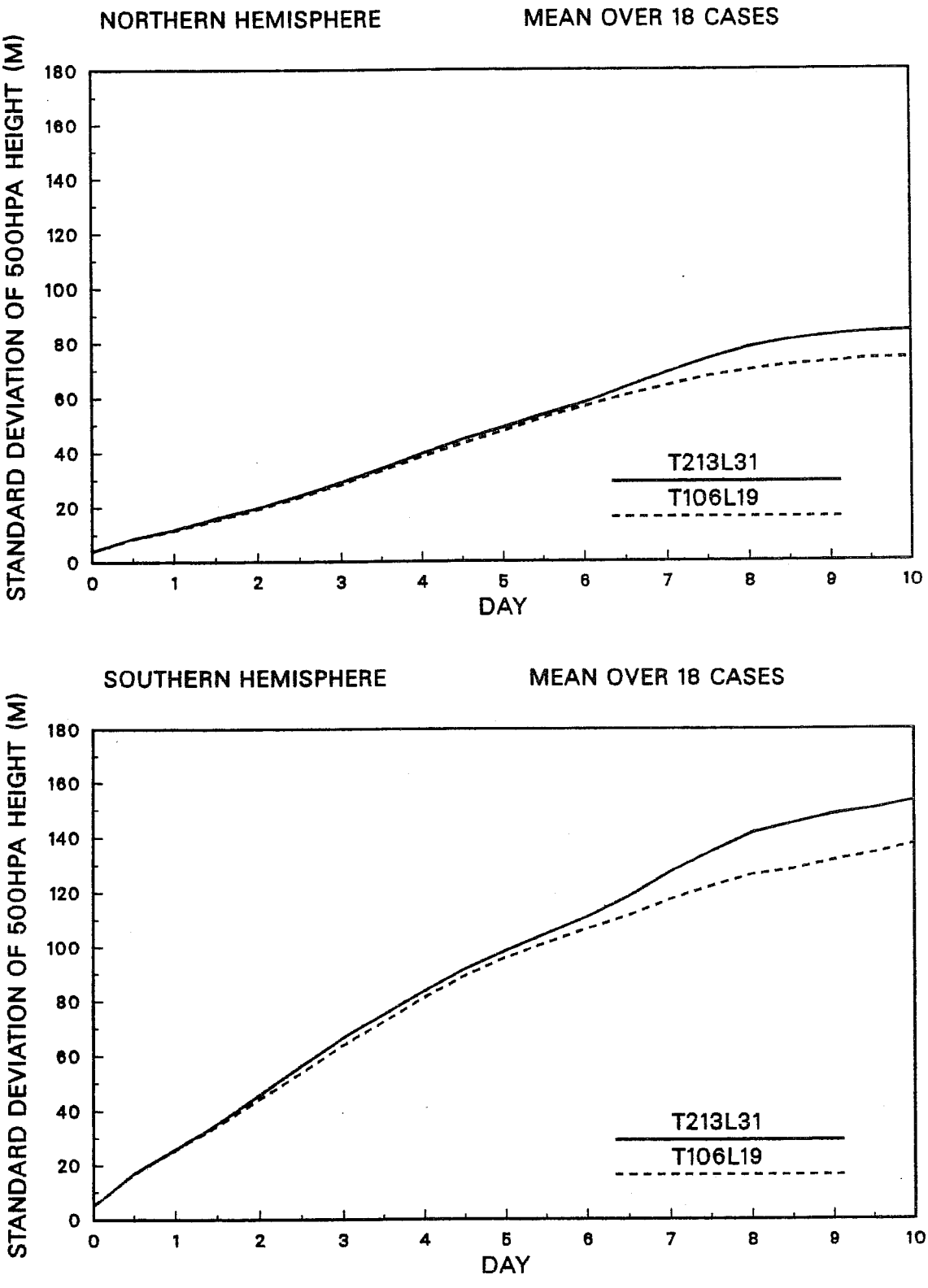

Fig. 22 Mean standard deviations of 500hPa height for T213/L31 (solid) and T106/L19 (dashed), computed over the extratropical northern (upper) and southern (lower) hemispheres, from daily forecasts for the period 11-28 July 1991.

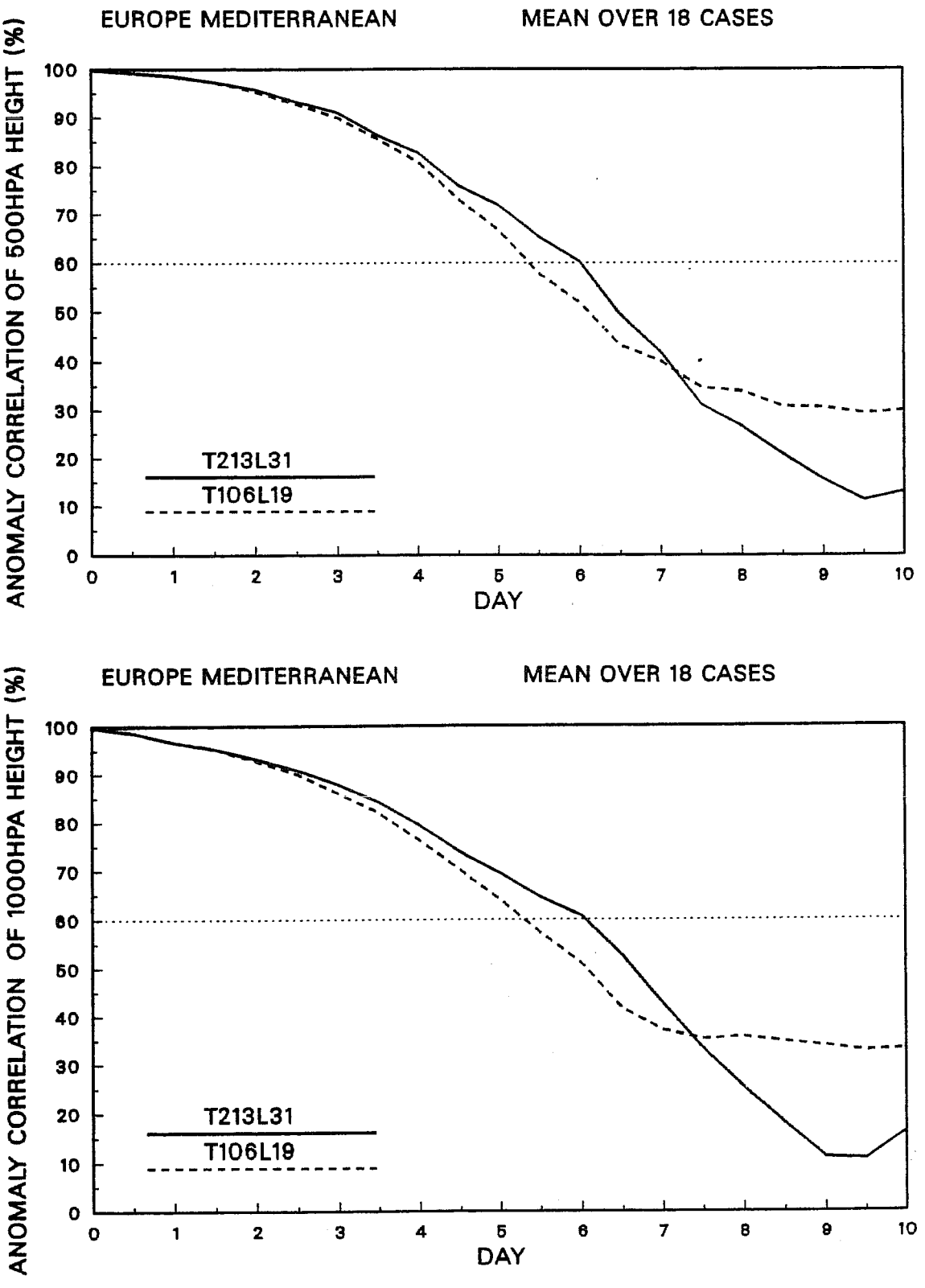

Fig. 23 Mean anomaly correlations of 500hPa (upper) and 1000hPa (lower) height for T213/L31 (solid) and T106/L19 (dashed), computed over the European region, from daily forecasts for the period 11-28 July 1991.

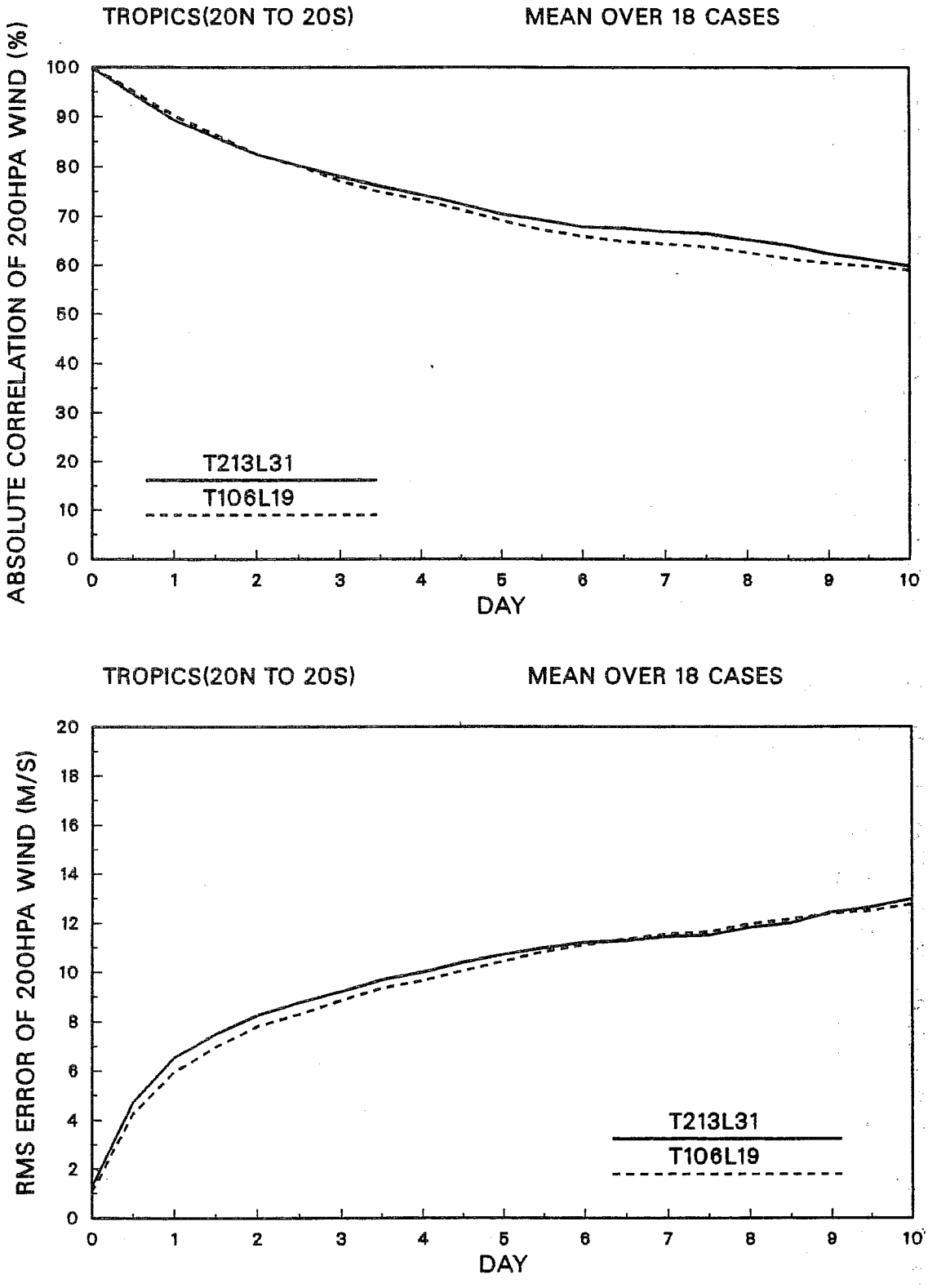

Fig. 24 Mean absolute correlations (upper) and rms errors (lower) of 200hPa vector wind for T213/L31 (solid) and T106/L19 (dashed), computed over the tropics, from daily forecasts for the period 11-28 July 1991.

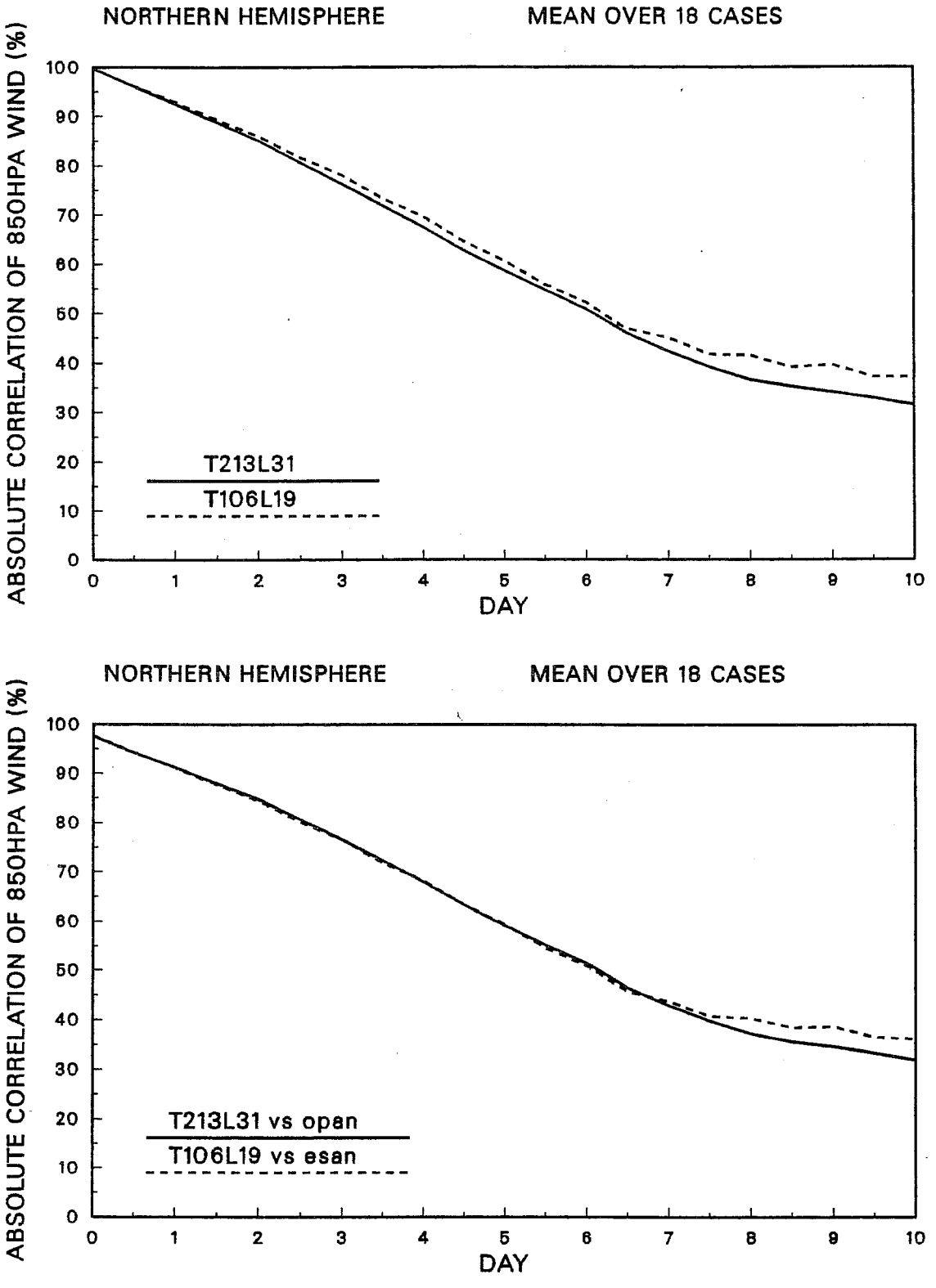

Fig. 25 Mean absolute correlations of 850hPa vector wind for T213/L31 (solid) and T106/L19 (dashed), computed over the extratropical northern hemisphere, from daily forecasts for the period 11-28 July 1991.
Upper plot: T213/L31 forecasts vs T213/L31 analyses.
T106/L19 forecasts vs T106/L19 analyses.
Lower plot: T213/L31 forecasts vs T106/L19 analyses.
T106/L19 forecasts vs T213/L31 analyses.

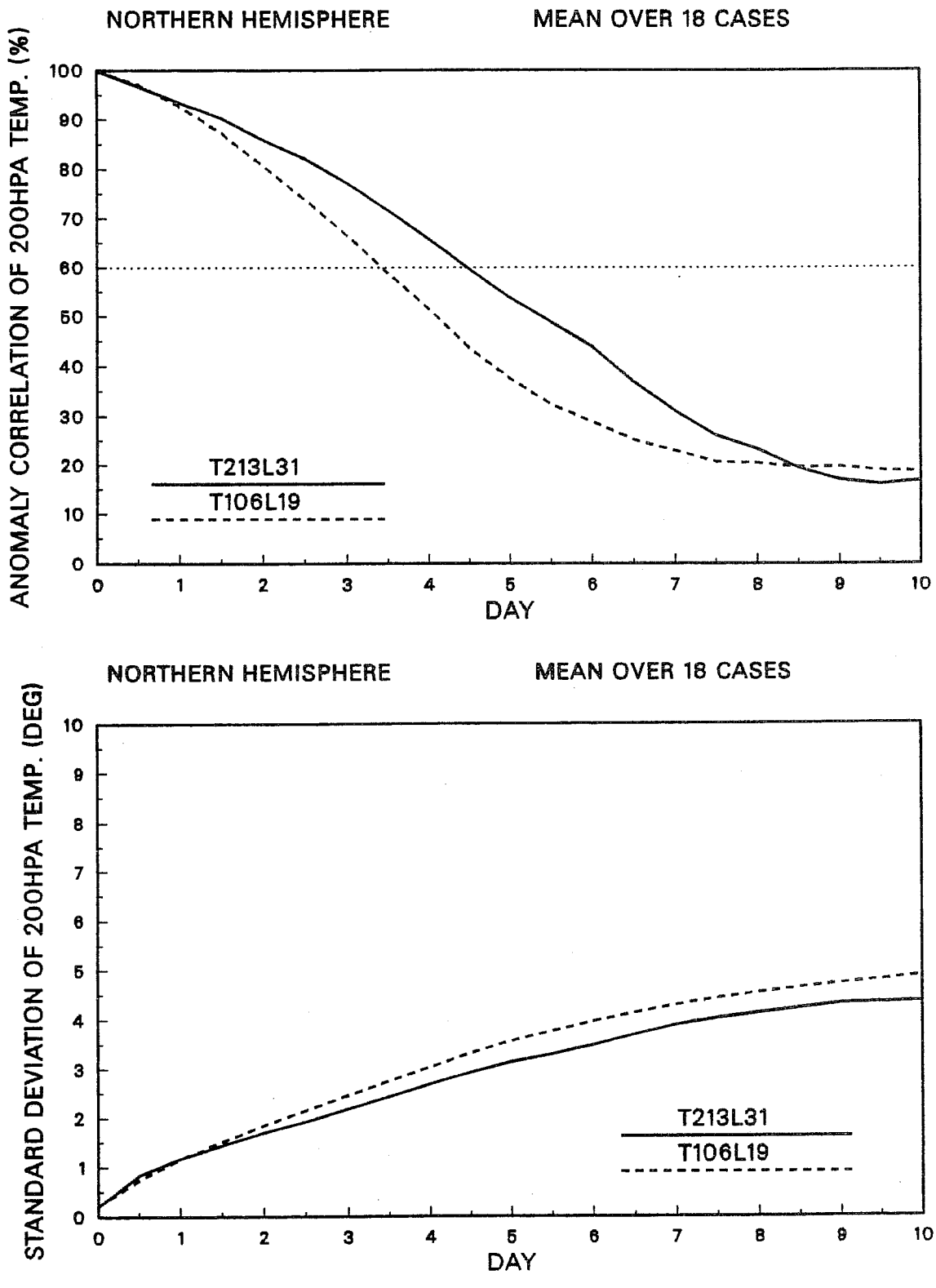

Fig. 26 Mean anomaly correlations (upper) and standard deviations (lower) of 200hPa temperature for T213/L31 (solid) and T106/L19 (dashed), computed over the extratropical northern hemisphere, from daily forecasts for the period 11-28 July 1991.

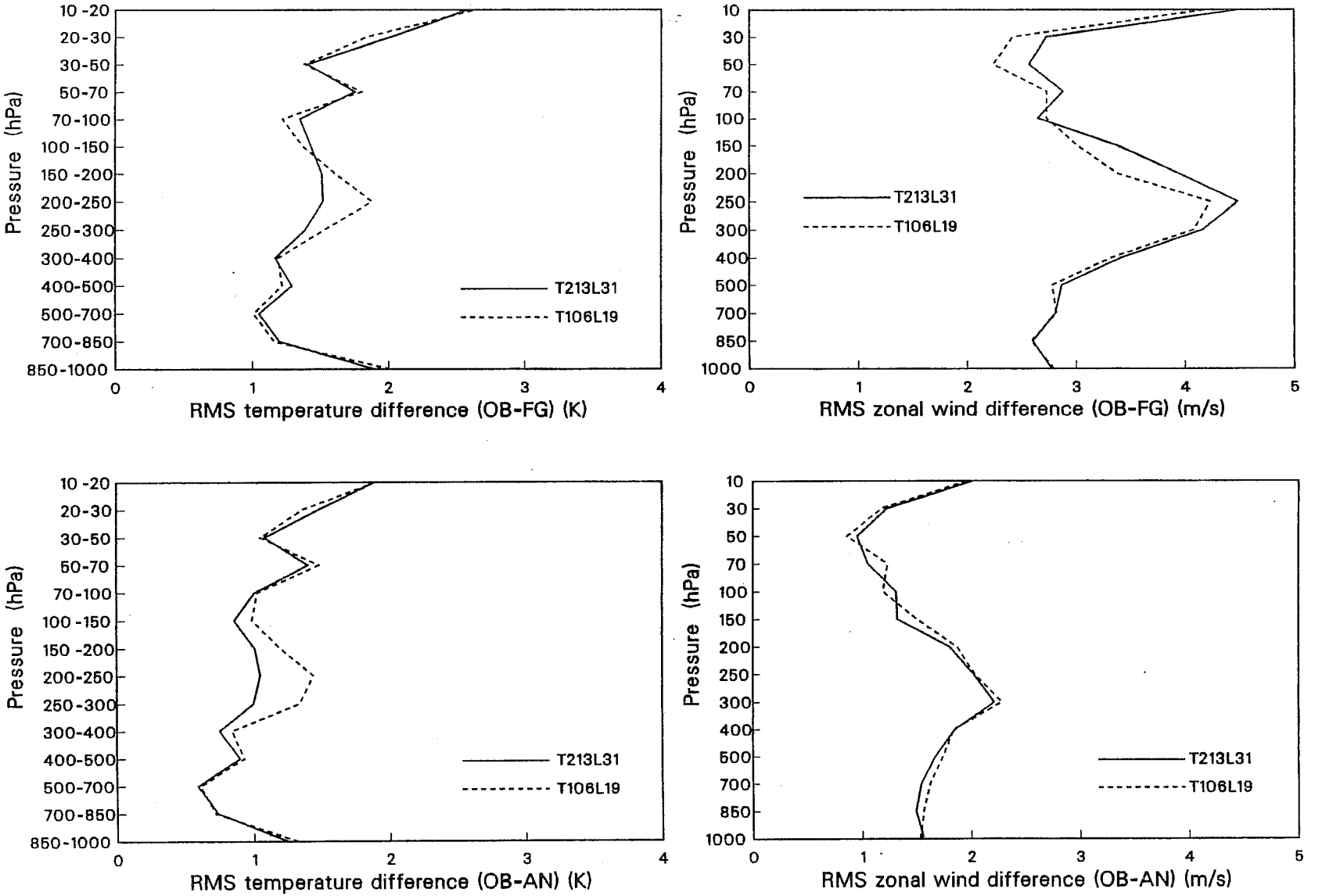

Fig. 27 Root-mean square fits of radiosonde observations over the extratropical northern hemisphere to first-guess (upper) and analyzed (lower) fields for layer-mean temperature (left) and the zonal wind component (right), for T213/L31 (solid) and T106/L19 (dashed), based on 12UTC data for the period 23-31 July 1991.